공학석사학위논문

# Initial design approach of CubeSat systems through mission analysis and operation simulation

## 임무 분석 및 운용 모사를 통한 큐브위성 초기설계 접근 방법

2013년 2월

서울대학교 대학원

기계항공공학부

박 지 현

# Initial design approach of CubeSat systems through mission analysis and operation simulation

# 임무 분석 및 운용 모사를 통한 큐브위성 초기설계 접근 방법

지도교수 정 인 석

이 논문을 공학석사학위논문으로 제출함

**2013년 2월**


서울대학교 대학원

기계항공공학부

박 지 현


박지현의 공학석사학위논문을 인준함

**2013년 2월**

위 원 장 : ____________________

부 위 원 장 : ____________________

위 원 : ____________________

# Abstract

## Initial design approach of CubeSat systems through mission analysis and operation simulation

Ji Hyun Park
Department of Aerospace Engineering
The Graduate School
Seoul National University

This study presents an initial design approach method for CubeSats. The study focuses on the pre-phase A procedure technical feasibility assessment. The pre-phase A procedure is important for a successful proposal and project. By introducing a simple mission analysis and operation simulation method and joining pre-phase A with a table based initial design approach, resources can be efficiently allocated.

The study uses Cowell's method with perturbing acceleration due to geopotential, atmospheric drag, solar radiation pressure, and third body. Space environment is modeled for ephemerides, rotational elements, eclipse, and atmospheric density.

With initial design, using the presented basic design table, and with top-level requirements, pre-phase A procedure of technical feasibility assessment for SNUSAT-1 is performed using the introduced orbit simulation method. As a result, initial design is given for SNUSAT-1.

*Keywords*: CubeSat, Initial Design, Pre-Phase A, Design Table, Mission Analysis, Operation Simulation
*Student Number*: 2011-20709

# Table of Contents

# List of Tables

# List of Figures

# List of Symbols

**Alphabet**

$a$: Semimajor axis of an orbit
$C_n^m$: Cosine term of the spherical harmonic coefficients
$\bar{C}_n^m$: Fully normalized cosine term of the spherical harmonic coefficients
$C_D$: Drag coefficient
$C_R$: Coefficient of reflectivity
$e$: Eccentricity of an orbit
$G$: Gravitational constant
$i$: Inclination of an orbit
$I_b$: Y-axis moment of inertia of the satellite
$I_w$: Moment of inertia of rotating mass of a reaction wheel
$M_\oplus$: Mass of Earth
$\vec{n}$: Unit vector normal to a surface
$\vec{r}$: Position of a satellite in the inertial coordinate
$\dot{\vec{r}}$: Velocity of a satellite in the inertial coordinate
$\ddot{\vec{r}}$: Acceleration of a satellite in the inertial coordinate
$\ddot{\vec{r}}_{\mathrm{geopotential}}$: Acceleration due to geopotential of a satellite in the inertial coordinate
$\ddot{\vec{r}}_{drag}$: Acceleration due to atmospheric drag of a satellite in the inertial coordinate
$\ddot{\vec{r}}_{\mathrm{SRP}}$: Acceleration due to solar radiation pressure of a satellite in the inertial coordinate
$\ddot{\vec{r}}_{\mathrm{third\ body}}$: Acceleration due to third body of a satellite in the inertial coordinate
$\vec{e}_\odot$: Unit vector directing the Sun from the satellite
$E_\odot$: Shadow function
$P_\odot$: Solar radiation pressure
$P_n$: Legendre polynomial of degree $n$
$P_n^m$: Associated Legendre function of degree $n$ and order $m$
$\bar{P}_n^m$: Fully normalized associated Legendre function of degree $n$ and order $m$
$r_\odot$: Geocentric distance of the Sun
$S_n^m$: Sine term of the spherical harmonic coefficients
$\bar{S}_n^m$: Fully normalized sine term of the spherical harmonic coefficients

$T_{\mathrm{m}}$: Nighttime minimum exospheric temperature
$T_{1/2}$: Mean exospheric temperature
$T_{\mathrm{M}}$: Daytime maximum exospheric temperature
$U$: Earth's gravity potential
$v_r$: Relative velocity of the satellite to the atmosphere
$x$: $\hat{x}$ component of the inertial satellite position vector
$y$: $\hat{y}$ component of the inertial satellite position vector
$z$: $\hat{z}$ component of the inertial satellite position vector

**Greek**
$\alpha$: Right ascension
$\delta$: Declination
$\varepsilon$: Obliquity of the ecliptic
$\varepsilon_{\odot}$: Coefficient of reflectivity
$\theta$: Greenwich apparent sidereal time
$\theta_m$: Greenwich mean sidereal time
$\theta_{\odot}$: Inclined angle between $\vec{e}_{\odot}$ and $\vec{n}$
$\vartheta$: Geocentric colatitude
$\rho$: Geocentric distance
$\rho_a$: Atmospheric density
$\lambda$: Geocentric longitude
$\mu$: Standard gravitational parameter of Earth (398,600.4418 $km^3s^{-2}$)
ν: True anomaly of an orbit
$\varphi$: Geocentric latitude
$\vec{\omega}_{\oplus}$: Angular velocity of the atmosphere
$\omega$: Argument of periapsis of an orbit
$\omega_b$: Rotation speed of the satellite
$\omega_w$: Rotation rpeed of the reaction wheel
$\bar{\Delta}$: Scaling factor
$\Delta\psi$: Periodic shift of the vernal equinox
Ω: Right ascension of the ascending node of an orbit
$\Omega_b$: Angular momentum of the satellite

# 1. Introduction

NanoSatellite, CubeSat, and its subsystems will be briefly introduced for basic information in why some of the design parameters are set in a certain way. The definition of NanoSatellite varies but it usually refers to satellites that are 1~10 kg. A CubeSat is a standardized NanoSatellite that uses COTS (Commercial-Off-The-Shelf) components with $100 \times 100 \times 113.5\ mm^3$ and 1.33 kg [California Polytechnic State University, 2009] being a single unit. Due to the use of COTS components and its small size, the development budget of CubeSat became as low as in the order of 1/1000 of a commercial satellite, and the development period became as short as about 1~2 years. Since, universities started to develop CubeSats, and eventually brought a boost in advancement of NanoSatellite technology.

This study presents a design method of early stages of CubeSat development, especially before and during the project proposal process also known as pre-phase A [NASA, 2007].

Pre-phase A of a design process is a phase where the feasibility of a certain mission, whether it is scientific or technical, is checked prior to the actual project. This phase can be said to be the most important process, since the whole process starting before the mission proposal to the beginning of operation is kept short (~2.5 years), especially for universities working on CubeSats, pre-phase A which occurs before the proposal is critical. A systematic pre-phase A process will lead to a successful project technically and scientifically.

According to the NASA Systems Engineering Handbook [2007], concept studies are performed in pre-phase A for selection of new programs. It includes mission justification, requirements identification, cost-schedule-risk estimates, mission feasibility assessment, and etc.

This study focuses on the pre-phase A process of technical evaluating the mission feasibility for operation concepts of CubeSats. Initial design approach is performed according to top-level requirements of a system, using a proposed basic design table. Since CubeSat is a standardized NanoSatellite, the components of subsystems are somewhat similar to each other in mass or in power consumption unless specific requirements exist for special missions. The basic design table is a survey of existing components that aids initial design process to give a brief idea of the design budget. The design is then assessed through operation simulation using numerical methods.

In chapter 2, the numerical methods for operation simulation are introduced. Cowell's method is used with perturbing acceleration due to geopotential, atmospheric drag, solar radiation pressure, and third body is considered.

In chapter 3, space environment modeling methods are introduced. The numerical methods and space environment modeling methods are validated throughout the chapter.

In chapter 4, CubeSat subsystems are introduced and a simplified initial design method is proposed. The design is approached using tables that are based on commercial products available for CubeSats organized in purpose of usage and applicable size units.

In chapter 5, an example of the pre-phase A is shown where the proposed design method is applied for SNUSAT-1, and feasibility is checked using the numerical methods.

# 2. Numerical Methods

This chapter introduces the numerical methods used for operation simulation. Cowell's method is used, which considers perturbing acceleration additionally to two-body orbital mechanics. Geopotential, atmospheric drag, solar radiation pressure, and third body, which are the largest perturbing sources for low Earth orbit [Montenbruck et al., 2000, p. 55] are considered. Since these perturbing forces cannot be directly calculated, they are numerically integrated using the fourth order Runge-Kutta method.

## 2.1. Equation of Motion

### 2.1.1. Cowell's Method

Cowell's method is adopted in this study for the numerical orbit analysis. Cowell's method is a special perturbation method, which includes necessary perturbing acceleration in the equation of motion and direct numerical integration is performed. Using Cowell's method, the states of the satellite can be obtained for every integration step. Cowell's method can be written as

$$\ddot{\vec{r}} = -\frac{\mu}{|\vec{r}|^3}\vec{r} + \ddot{\vec{r}}_{geopotential} + \ddot{\vec{r}}_{drag} + \ddot{\vec{r}}_{SRP} + \ddot{\vec{r}}_{third\ body}, \tag{2.1}$$

where the terms on the right-hand side are acceleration due to universal gravitation, geopotential, atmospheric drag, solar radiation pressure, third body, which are the main perturbing sources for low Earth orbit. Other terms may include Earth radiation pressure, Earth tides, general relativity, and etc. However, just the main perturbations mentioned above are considered, since this study focuses on the feasibility assessment, unless the mission involved require high precession orbit knowledge.

Acceleration due to geopotential, atmospheric drag, solar radiation pressure, and third body is further dealt in detail in the following sections.

### 2.1.2. Geopotential

Since Earth is not actually a point mass, distributed mass of Earth exerts perturbing acceleration on the satellite about the center of its orbit. By taking a mass element and integrating them gives a generalized Earth's gravity potential. The equation is given as in Montenbruck and Gill [2000, Eq. 3.4]

$$U = G\int \frac{\rho(\vec{s})d^3\vec{s}}{|\vec{r}-\vec{s}|}. \tag{2.2}$$

The inverse of the distance term can be further expanded into a series of Legendre polynomials as the following.

$$\frac{1}{|\vec{r}-\vec{s}|} = \frac{1}{r}\sum_{n=0}^{\infty}\left(\frac{s}{r}\right)^n P_n(\cos\gamma), \tag{2.3}$$

$$\cos\gamma = \frac{\vec{r}\cdot\vec{s}}{rs}, \tag{2.4}$$

where $P_n(\cos\gamma)$ is the Legendre polynomial of degree $n$.

Introducing $\lambda$ and $\varphi$ as the geocentric longitude and latitude of $\vec{r}$, $\lambda'$ and $\varphi'$ as the geocentric longitude and latitude of $\vec{s}$, and using the addition theory of Legendre polynomials, $P_n(\cos\gamma)$ can be written as

$$P_n(\cos\gamma) = \sum_{m=0}^{n}(2-\delta_m)\frac{(n-m)!}{(n+m)!}P_n^m(\sin\varphi)P_n^m(\sin\varphi')\cos(m(\lambda-\lambda')), \tag{2.5}$$

where $P_n^m(\sin\varphi)$ is the associated Legendre polynomial of degree $n$ and order $m$.

Then, defining the spherical harmonic coefficients $C_n^m$ and $S_n^m$ as

$$C_n^m = \frac{2-\delta_m}{M_\oplus}\frac{(n-m)!}{(n+m)!}\int\left(\frac{s}{R_\oplus}\right)^n P_n^m(\sin\varphi')(\cos m\lambda')\rho(\vec{s})d^3\vec{s}, \tag{2.6}$$

$$S_n^m = \frac{2-\delta_m}{M_\oplus}\frac{(n-m)!}{(n+m)!}\int\left(\frac{s}{R_\oplus}\right)^n P_n^m(\sin\varphi')(\sin m\lambda')\rho(\vec{s})d^3\vec{s}, \tag{2.7}$$

Earth's gravity potential can be written as

$$\mathrm{U}(r,\varphi,\lambda) = \frac{GM_\oplus}{r}\sum_{n=0}^{\infty}\sum_{m=0}^{n}\left(\frac{R_\oplus}{r}\right)^n \bar{P}_n^m(\sin\varphi)(\bar{C}_n^m\cos m\lambda + \bar{S}_n^m\sin m\lambda). \tag{2.8}$$

Then, perturbing acceleration can be obtained from the gradient of the gravity potential, which is given as

$$\ddot{\vec{r}} = \vec{\nabla} U = \frac{\partial U}{\partial r}\vec{e}_r + \frac{1}{r}\frac{\partial U}{\partial \varphi}\vec{e}_\varphi + \frac{1}{r\cos\varphi}\frac{\partial U}{\partial \lambda}\vec{e}_\lambda, \tag{2.9}$$

$$\frac{\partial U}{\partial r} = -\frac{GM_\oplus}{r^2}\sum_{n=0}^{\infty}\sum_{m=0}^{n}\left(\frac{R_\oplus}{r}\right)^n (n+1)\bar{P}_n^m(\sin\varphi)(\bar{C}_n^m\cos m\lambda + \bar{S}_n^m \sin m\lambda), \tag{2.10}$$

$$\frac{\partial U}{\partial \varphi} = \frac{GM_\oplus}{r}\sum_{n=0}^{\infty}\sum_{m=0}^{n}\left(\frac{R_\oplus}{r}\right)^n \frac{\partial \bar{P}_n^m(\sin\varphi)}{\partial \varphi}(\bar{C}_n^m\cos m\lambda + \bar{S}_n^m \sin m\lambda), \tag{2.11}$$

$$\frac{\partial U}{\partial \lambda} = \frac{GM_\oplus}{r}\sum_{n=0}^{\infty}\sum_{m=0}^{n}\left(\frac{R_\oplus}{r}\right)^n \bar{P}_n^m(\sin\varphi) m(-\bar{C}_n^m\sin m\lambda + \bar{S}_n^m \cos m\lambda), \tag{2.12}$$

where $\bar{P}_n^m(\sin\varphi)$ is fully normalized associated Legendre function of degree $n$ and order $m$, $\bar{C}_n^m$ and $\bar{S}_n^m$ are the fully normalized spherical harmonic coefficients, $GM_\oplus = \mu$ is the standard gravitational parameter of Earth, and $R_\oplus$ is the equatorial radius of Earth.

Note that the coordinate system is given in modified spherical coordinate using latitude instead of colatitude, where $\varphi = \pi/2 - \vartheta$.

In order to calculate the accelerations due to geopotential, the Associated Legendre function must be obtained. If $\varphi$ is defined so that it satisfies $\varphi = \pi/2 - \vartheta$, then it also satisfies $cos\,\vartheta = sin\,\varphi$ and thus

$$P_n^m(\cos\vartheta) = P_n^m(\sin\varphi). \tag{2.13}$$

Associated Legendre function is defined as

$$P_n^m(x) := (1-x^2)^{m/2}\frac{d^m P_n(x)}{dx^m}, \tag{2.14}$$

where $P_n(x)$ are the Legendre polynomials of degree $n$, which is defined as

$$P_n(x) := \frac{1}{2^n n!}\frac{d^n}{dx^n}(x^2-1)^n. \tag{2.15}$$

Due to the derivative term in the end of $P_n^m(x)$, $P_n^m(x) = 0$ for all $m > n$.

However, since $P_n^m(\sin\varphi)$ becomes numerically unstable for high degree and order, and since geopotential spherical harmonic coefficients are normalized, fully normalized associated Legendre function, $\bar{P}_n^m(\sin\varphi)$, is used. $P_n^m(\sin\varphi)$ is normalized as

$$\bar{P}_n^m(\sin\varphi) = \sqrt{\frac{k(2n+1)(n-m)!}{(n+m)!}}P_n^m(\sin\varphi), \tag{2.16}$$

where $k = 1$ for $m = 0$ and $k = 2$ for $m > 0$.

$\bar{P}_n^m(\sin\varphi)$ can be obtained from one of many recursions summarized by Holmes and Featherstone [2002, pp. 281-282] as

$$\bar{P}_n^n(sin\,\varphi) = cos\,\varphi\sqrt{\frac{2n+1}{2n}}\,\bar{P}_{n-1}^{n-1}(sin\,\varphi), \qquad (2.17)$$

for sectoral (i.e., $n = m$) $\bar{P}_n^n(sin\,\varphi)$ and

$$\bar{P}_n^m(\sin\varphi) = a_n^m \sin\varphi\,\bar{P}_{n-1}^m(\sin\varphi) - b_n^m \bar{P}_{n-2}^m(\sin\varphi), \qquad (2.18)$$

$$a_n^m = \sqrt{\frac{(2n-1)(2n+1)}{(n-m)(n+m)}}, \qquad (2.19)$$

$$b_n^m = \sqrt{\frac{(2n+1)(n+m-1)(n-m-1)}{(n-m)(n+m)(2n-3)}}, \qquad (2.20)$$

for non-sectoral ((i.e., $n > m$) $\bar{P}_n^n(sin\,\varphi)$ with $\bar{P}_0^0(\sin\varphi) = 1$, $\bar{P}_1^0(sin\,\varphi) = sin\,\varphi\sqrt{3}$, and $\bar{P}_1^1(sin\,\varphi) = cos\,\varphi\,\sqrt{3}$.

In order to obtain geopotential term $\frac{\partial U}{\partial \varphi}$, $\frac{\partial \bar{P}_n^m(\sin\varphi)}{\partial \varphi}$ must be further calculated, in which the methods are summarized by Bosch [2000, p. 656] as

$$cos\,\varphi\frac{\partial \bar{P}_n^m(\sin\varphi)}{\partial\varphi} = m\sin\varphi\,\bar{P}_n^m(\sin\varphi) - cos\,\varphi\,\bar{P}_n^{m+1}(\sin\varphi), \qquad (2.21)$$

$$cos\,\varphi\frac{\partial \bar{P}_n^m(\sin\varphi)}{\partial\varphi} = n\sin\varphi\,\bar{P}_n^m(\sin\varphi) - (n+m)\bar{P}_{n-1}^m(\sin\varphi), \qquad (2.22)$$

or as

$$2\frac{\partial \bar{P}_n^m(\sin\varphi)}{\partial\varphi} = \sqrt{(n+m)(n-m+1)}\bar{P}_n^{m-1}(\sin\varphi) - \sqrt{(n+m+1)(n-m)}\bar{P}_n^{m+1}(\sin\varphi), \qquad (2.23)$$

for $1 < m < n$, with

$$\frac{\partial \bar{P}_0^0(\sin\varphi)}{\partial\varphi} \equiv 0, \qquad (2.24)$$

$$\frac{\partial \bar{P}_n^0(\sin\varphi)}{\partial\varphi} = -\sqrt{\frac{n(n+1)}{2}}\,\bar{P}_n^1(\sin\varphi), \qquad (2.25)$$

for $m = 0$,

$$\frac{\partial \bar{P}_1^1(\sin\varphi)}{\partial\varphi} = \bar{P}_1^0(\sin\varphi), \tag{2.26}$$

$$2\frac{\partial \bar{P}_n^1(\sin\varphi)}{\partial\varphi} = \sqrt{n(n+m)}\bar{P}_n^0(\sin\varphi) - \sqrt{(n-1)(n+2)}\bar{P}_n^2(\sin\varphi), \tag{2.27}$$

for $m = 1$, and

$$\frac{\partial \bar{P}_n^n(\sin\varphi)}{\partial\varphi} = \sqrt{\frac{n}{2}}\bar{P}_n^{n-1}(\sin\varphi), \tag{2.28}$$

for $n = m > 1$.

Since geopotential acceleration is given in an Earth-fixed coordinate system, it must be transformed into the inertial coordinate system in order to perform orbit integration.

The modified spherical coordinate is transformed into Cartesian coordinates using the following transformation matrix, which is obtained from basic trigonometry. Nutation and precision is neglected in the transformation matrix.

$$\begin{bmatrix}\hat{x}\\ \hat{y}\\ \hat{z}\end{bmatrix} = \begin{bmatrix}\frac{x}{\sqrt{x^2+y^2+z^2}} & \frac{xz}{\sqrt{x^2+y^2}\sqrt{x^2+y^2+z^2}} & \frac{-y}{\sqrt{x^2+y^2}}\\ \frac{y}{\sqrt{x^2+y^2+z^2}} & \frac{yz}{\sqrt{x^2+y^2}\sqrt{x^2+y^2+z^2}} & \frac{x}{\sqrt{x^2+y^2}}\\ \frac{z}{\sqrt{x^2+y^2+z^2}} & \frac{-\sqrt{x^2+y^2}}{\sqrt{x^2+y^2+z^2}} & 0\end{bmatrix}\begin{bmatrix}\hat{r}\\ \hat{\varphi}\\ \hat{\lambda}\end{bmatrix}. \tag{2.29}$$

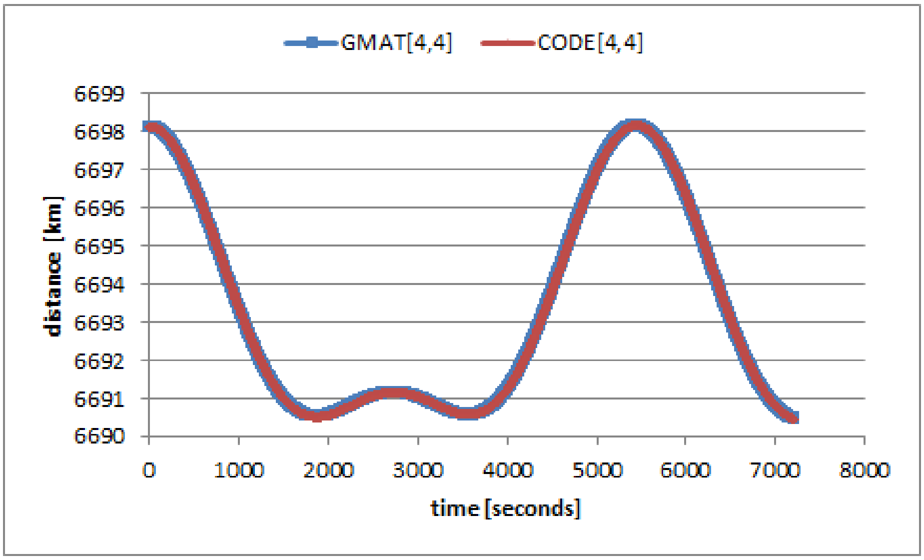


**Figure 1** Comparison result of geopotential perturbation with GMAT

For the spherical harmonic coefficients, GRACE Gravity Model, GGM03C is used throughout the study, whereas EGM96 is used for geopotential validation with NASA General Mission Analysis Tool (GMAT). The comparison with only geopotential considered as perturbation results are shown in Figure 1.

### 2.1.3. Atmospheric Drag

Atmospheric drag is the largest non-gravitational force acting on the satellite for Earth orbits. The equation for atmospheric drag is given as

$$\ddot{\vec{r}}_{drag} = -\frac{1}{2} C_D \frac{A}{m} \rho_a v_r^2 \frac{\vec{v}_r}{|\vec{v}_r|}, \tag{2.30}$$

where $C_D$ is the drag coefficient, normally 2.2 for CubeSats, $A$ is the cross-sectional area of the satellite, $m$ is the mass of the satellite, $\rho_a$ is the density of the atmosphere, and $\vec{v}_r$ is the relative velocity of the satellite to the atmosphere.

It is hard to estimate the drag coefficient, since the drag coefficient depends on the shape, surface material, chemical constituents of the atmosphere, and the temperature. Also, the effect of altitude should not be left out since the drag coefficient does change according to the Knudsen number, which is affected by the altitude. As the orbit decays and the altitude get lower and thus the Knudsen number decreases, the atmosphere is seen as a hypersonic continuum flow, where the drag coefficient drops down to near 1.

The relative velocity of the satellite to the atmosphere is simplified by assuming the atmosphere rotates with the Earth. Then, the relative velocity of the satellite to the atmosphere can be written as

$$\vec{v}_r = \vec{v} - \vec{\omega}_\oplus \times \vec{r}, \tag{2.31}$$

where $\vec{v}$ is the velocity of the satellite, $\vec{\omega}_\oplus$ is the angular velocity of the atmosphere, and $\vec{r}$ is the position vector of the satellite. Taking the mean sidereal day (23 hours 56 minutes 4.093 seconds), the size of the angular velocity of the atmosphere is calculated to be about $7.29212 \times 10^{-5}\, rad/s$. Study on global atmospheric wind model exists by Hedin et al. [1988], however, this study adopts the assumption of co-rotating atmosphere. If the mission of the satellite requires higher precision in atmospheric drag modeling, the study of Hedin et al. should be considered.

The atmospheric density $\rho_a$ is one of the most critical parameter for assessing atmospheric drag. Atmospheric density depends not only on the many models such as Jacchia models or MSIS models, but also depends on the parameters within the models such as exospheric temperature or geomagnetic index. Some of the atmospheric models were summarized as shown in Figure **2** by Vallado [2007].

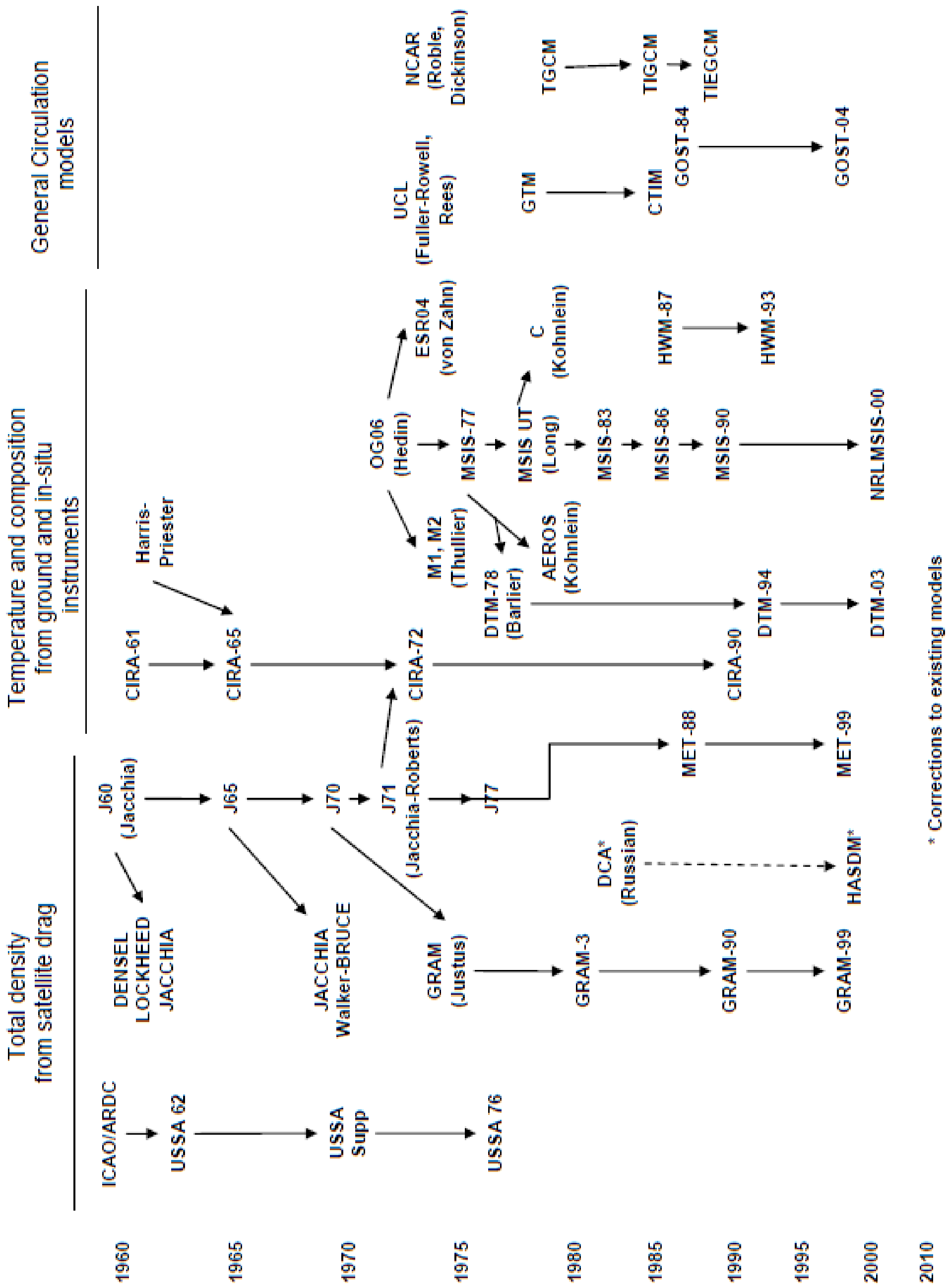


**Figure 2** Summary of atmosphere models [Vallado, 2007]

In this study, a simplified Jacchia 77 model is used. The Jacchia 77 models solely take the exospheric temperature, which is a function of the 10.7cm band solar flux $F_{10.7}$ and the geomagnetic index $K_p$. According to Jacchia [1977, p. 16], the exospheric temperature is affected by seasonal changes, solar cycles, daily changes, geomagnetic activities, and semiannual variations. However in this study, only the solar cycle is considered as the initial value for calculating the initial exospheric temperature, taking the mean exospheric temperature $T_{1/2}$ between the nighttime minimum $T_m$ and the daytime maximum $T_M$. The mean exospheric temperature is given as

$$T_{1/2} = 5.48\bar{F}^{0.8} + 101.8F^{0.4}, \tag{2.32}$$

where $\bar{F}$ is the average of $F$ over six solar rotations, being 142 days. If the mission requires higher precision over atmospheric drag, not only should daily-seasonal-semiannual effect, geomagnetic index, and space weather be considered in the Jacchia model, but also other models should be used. Detail on the Jacchia model is further described in section 3.5.

### 2.1.4. Solar Radiation Pressure

Solar radiation pressure is an acceleration source due to absorption or reflection of photons that come from the Sun. The equation for solar radiation pressure is given as [Montenbruck, 2000, Eq. 3.73]

$$\ddot{\text{r}}_{SRP} = -P_\odot \frac{1AU^2}{r_\odot^2}\frac{A}{m}\cos(\theta_\odot)\left[(1-\varepsilon_\odot)\vec{e}_\odot + 2\varepsilon_\odot\cos(\theta_\odot)\vec{n}\right], \tag{2.33}$$

where the solar radiation pressure $P_\odot \approx 4.56 \times 10^{-6}\ Nm^{-2}$, $1\ AU \approx 1.49598 \times 10^8\ km$, $r_\odot$ is the geocentric distance of the Sun, $\vec{e}_\odot$ is the vector directing the Sun from the satellite, $\vec{n}$ is the vector normal to the surface $A$, $\theta_\odot$ is the inclined angle between $\vec{e}_\odot$ and $\vec{n}$, and $\varepsilon_\odot$ is the coefficient of reflectivity. If it is assumed that $\vec{n}$ points the sun, thus $\vec{n} = \vec{e}_\odot$, then $\cos(\theta_\odot) = 1$ and solar radiation pressure is simplified as

$$\ddot{\text{r}}_{SRP} = -P_\odot C_R \frac{A}{m}\frac{\vec{r}_\odot}{r_\odot^3}AU^2, \tag{2.34}$$

where the radiation pressure coefficient $C_R = 1 + \varepsilon_\odot \approx 1.21$ for CubeSats according to Table 1 given by van der Ha [1977, Table 2.1], since normally all sides of the CubeSats are basically covered by solar panels.

**Table 1** Coefficient of reflectivity and radiation pressure coefficient

| Components | $\varepsilon_\odot$ | $1-\varepsilon_\odot$ | $C_R = 1+\varepsilon_\odot$ |
|---|---|---|---|
| Solar panel | 0.21 | 0.79 | 1.21 |
| High-gain Antenna | 0.30 | 0.70 | 1.30 |
| Solar Sail | 0.88 | 0.12 | 1.88 |

Since solar radiation pressure exists due to the Sun, solar radiation pressure if affected by the shadows, and the solar radiation pressure can be rewritten as

$$\ddot{\mathrm{r}}_{SRP} = -E_\odot P_\odot \frac{1AU^2}{r_\odot^2}\frac{A}{m}\cos(\theta_\odot)\left[(1-\varepsilon_\odot)\vec{e}_\odot + 2\varepsilon_\odot\cos(\theta_\odot)\vec{n}\right], \tag{2.35}$$

where $E_\odot$ is the shadow function, further described in section 3.4.

### 2.1.5. Third Body Perturbation

Newton's law of universal gravitation state that an object with mass $M$ attracts an object with mass $m$ with a force

$$\vec{F}_g = -\frac{GMm}{r^2}\frac{\vec{r}}{r}, \tag{2.36}$$

where $G$ is the gravitational constant, and $\vec{r}$ is the vector pointing from $m$ to $M$. The equation can be further expanded by taking $n$ bodies within a system into account with mass of $\mathrm{m}_n$ and rewriting the equation gives

$$\vec{F}_{gn} = -\frac{Gm_i m_n}{r_{ni}^3}\vec{r}_{ni}, \tag{2.37}$$

where $\vec{F}_{gn}$ is the force on $m_i$ by $m_n$, and $\vec{r}_{ni} = \vec{r}_i - \vec{r}_n$ is the vector pointing from $m_n$ to $m_i$. The vector sum $\vec{F}_g$ acting on $m_i$ can be expanded by adding all the elements in the system as

$$\vec{F}_g = -\frac{Gm_i m_1}{r_{1i}^3}\vec{r}_{1i} - \frac{Gm_i m_2}{r_{2i}^3}\vec{r}_{2i} - \cdots - \frac{Gm_i m_n}{r_{ni}^3}\vec{r}_{ni} = -Gm_i\sum_{j=1,j\neq i}^{n}\frac{m_j}{r_{ji}^3}\vec{r}_{ji}, \tag{2.38}$$

and since $\vec{F}_g = m_i\ddot{\vec{r}}_i$,

$$\ddot{\vec{r}}_i = -G \sum_{j=1, j\neq i}^{n} \frac{m_j}{r_{ji}^3} \vec{r}_{ji}. \tag{2.39}$$

Letting $m_1$ be the Earth and $m_2$ be the satellite,

$$\ddot{\vec{r}}_1 = -G \sum_{j=2}^{n} \frac{m_j}{r_{j1}^3} \vec{r}_{j1}, \tag{2.40}$$

$$\ddot{\vec{r}}_2 = -G \sum_{j=1, j\neq 2}^{n} \frac{m_j}{r_{j2}^3} \vec{r}_{j2}, \tag{2.41}$$

and from $\vec{r}_{12} = \vec{r}_2 - \vec{r}_1$,

$$\ddot{\vec{r}}_{12} = \ddot{\vec{r}}_2 - \ddot{\vec{r}}_1, \tag{2.42}$$

$$\ddot{\vec{r}}_{12} = -G \sum_{j=1, j\neq 2}^{n} \frac{m_j}{r_{j2}^3} \vec{r}_{j2} - \left(-G \sum_{j=2}^{n} \frac{m_j}{r_{j1}^3} \vec{r}_{j1}\right), \tag{2.43}$$

$$\ddot{\vec{r}}_{12} = \left(-\frac{Gm_1}{r_{12}^3} \vec{r}_{12} - G \sum_{j=3}^{n} \frac{m_j}{r_{j2}^3} \vec{r}_{j2}\right) - \left(-\frac{Gm_2}{r_{21}^3} \vec{r}_{21} - G \sum_{j=3}^{n} \frac{m_j}{r_{j1}^3} \vec{r}_{j1}\right), \tag{2.44}$$

since $\vec{r}_{12} = -\vec{r}_{21}$,

$$\ddot{\vec{r}}_{12} = -\frac{G(m_1+m_2)}{r_{12}^3} \vec{r}_{12} - \sum_{j=3}^{n} Gm_j \left(\frac{\vec{r}_{j2}}{r_{j2}^3} - \frac{\vec{r}_{j1}}{r_{j1}^3}\right). \tag{2.45}$$

The first term on the right-hand side is the acceleration relative to the Earth, whereas the second term is the perturbing acceleration due to other objects in the solar system (i.e. the Moon, the Sun, and etc.). Thus, the second term is the third body perturbation, and in this study only the effect of the Moon and the Sun is considered, since they are the two largest source of acceleration according to Table 2 [Bate et al., 1971, Table 1.2-1].

**Table 2** Comparison of relative acceleration (in G's) for a 200 nm Earth Satellite [Bate et al., 1971, Table 1.2-1]

| Source | Acceleration in G's on 200 nm Earth Satellite |
|---|---|
| Earth | 0.89 |
| Sun | $6 \times 10^{-4}$ |
| Mercury | $2.6 \times 10^{-10}$ |
| Venus | $1.9 \times 10^{-8}$ |
| Mars | $7.1 \times 10^{-10}$ |
| Jupiter | $3.2 \times 10^{-8}$ |
| Saturn | $2.3 \times 10^{-9}$ |
| Uranus | $8 \times 10^{-11}$ |
| Neptune | $3.6 \times 10^{-11}$ |
| Moon | $3.3 \times 10^{-6}$ |

## 2.2. Numerical Integration

This study uses the Runge-Kutta method, since the Cowell's method requires numerical integration. The reason for need of a numerical integration method is due to time steps. Theoretically, integration is performed in infinitesimal time steps. However numerically, if the time steps are too small, it will increase the total number of computation and round off errors [Montenbruck et al., 2000, p. 123]. On the other hand, if the time step is too big, the integration will be performed only using the initial states, which in reality the states are continuously changing. One of the methods developed in order to overcome such problems is the Runge-Kutta method. Runge-Kutta method takes several trial steps within one integration step, which makes the integration higher order [Press et al., 2007, p. 907]. There are many kinds of Runge-Kutta methods regarding the number of trial steps and the coefficients for these trial steps. In this study particularly, fourth-order Runge-Kutta method, which is the classical Runge-Kutta method, is used.

The fourth-order Runge-Kutta method requires four steps, and therefore the increment for every step must be calculated, thus evaluation of the increment must be performed four times. The increments $k_i$ are given as

$$k_1 = hf(t_n, y_n), \tag{2.46}$$

$$k_2 = hf\left(t_n + {}^1\!/_2\, h, y_n + {}^1\!/_2\, k_1\right), \tag{2.47}$$

$$k_3 = hf\left(t_n + {}^1\!/_2\, h, y_n + {}^1\!/_2\, k_2\right), \tag{2.48}$$

$$k_4 = hf(t_n + h, y_n + k_3), \tag{2.49}$$

where $f(t_n, y_n)$ is the derivative of $y_n$ at time $t_n$ with $h$ being the integration time step. Then, $y_{n+1}$ is given as

$$y_{n+1} = y_n + (k_1 + 2k_2 + 2k_3 + k_4)/6 + O(h^5), \quad (2.50)$$

with a fifth order error $O(h^5)$. For use of the fourth-order Runge-Kutta method in orbit integration, the integration must be performed for $\dot{\vec{r}}_{n+1}$ and $\vec{r}_{n+1}$.

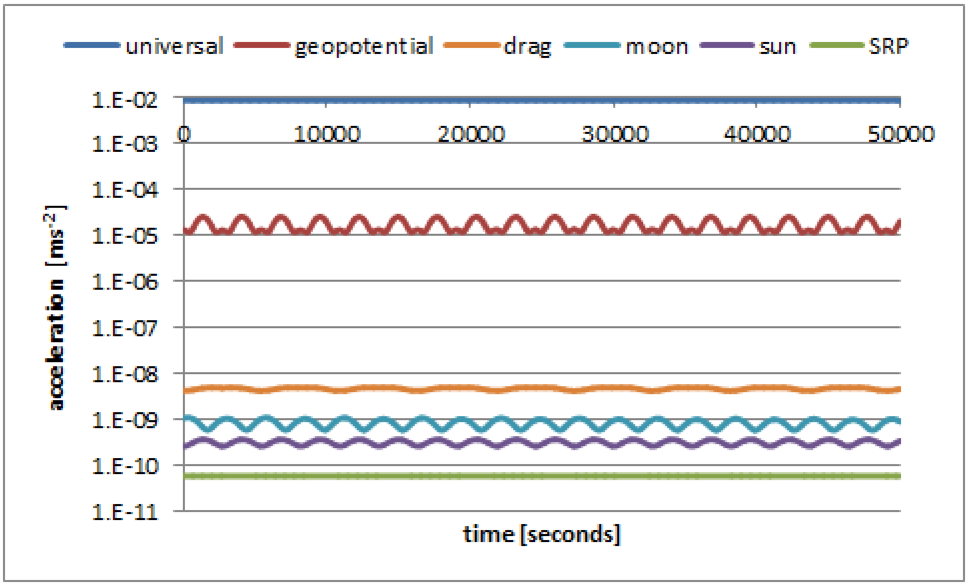


**Figure 3** Order of magnitude of acceleration sources

# 3. Space Environment Modeling

In this section, the space environment modeling methods are introduced. The space environment modeling includes the time and coordinate system, ephemerides, rotation elements, shadow (or solar eclipse), and the atmospheric model.

## 3.1. Time and Coordinate System (include initializing)

### 3.1.1. Time

For the analysis, many different kinds of time references are used. There are six major time references [Montenbruck et al., 2000, p. 158], which are Terrestrial Time, International Atomic Time, GPS Time, Greenwich Mean Sidereal Time, Universal Time and Coordinated Universal Time.

Terrestrial Time (TT) measures one day as 86,400 seconds, what we normally know as 24 hours a day. The Julian date obeys the time reference of TT with its Epoch, or the time origin, on 4713 BC January 1, 12h. Note that Terrestrial Time is equal to Terrestrial Dynamical Time (TDT) and Ephemeris Time (ET).

International Atomic Time (TAI) is related to Terrestrial Time, which follows the relation as

$$\mathrm{TAI} = \mathrm{TT} + 32.184. \tag{3.1}$$

Thus International Atomic Time and Terrestrial Time has the same time scale, however is just shifted by 32.184 seconds.

GPS Time (GPST) is also a time reference having the same time scale as the Terrestrial Time and the International Atomic Time. However, GPS Time has a time shift of 19 seconds, satisfying

$$\mathrm{GPST} = \mathrm{TT} + 19. \tag{3.2}$$

Greenwich Mean Sidereal Time is the angle between the mean vernal equinox and the Greenwich meridian. Sidereal Time measures a single rotation of the Earth as to the time difference of the sun rise. For Earth to see the next sun rise, Earth needs to rotate a small amount more that is has to rotate due to the revolution of Earth around the Sun. The length of one sidereal day, or the actual Earth's spin period is, $23^{\mathrm{h}}56^{m}4^{s}.091 \pm 0^{s}.005$. Both Greenwich Mean Sidereal Time and Universal Time cannot be converted as a function of the Terrestrial Time because Earth's rotation and revolution is irregular and cannot be predicted accurately. However, $0^{h}UT1$ is defined so it is equal to Greenwich Mean Sidereal Time value as

$$\mathrm{GMST}\left(0^{h}UT1\right) = 24110^{s}.54841 + 8640184^{s}.812866T_0 + 0^{s}.093104T_0^2 - 0^{s}.0000062T_0^3, \tag{3.3}$$

$$T_0 = \frac{JD\left(0^{h}UT1\right) - 2451545}{36525}, \tag{3.4}$$

where $JD\left(0^{h}UT1\right)$ is the Julian date 2451545.0 UT1. Precise Greenwich Mean Sidereal Time and Universal Time cannot be computed and must be derived from observations and measurements.

Coordinated Universal Time (UTC) is related to the International Atomic Times with an offset as

$$\mathrm{TAI} = \mathrm{UTC} + \Delta\mathrm{AT}, \tag{3.5}$$

where $\Delta\mathrm{AT}$ is the leap seconds. The leap second is controlled so that the Coordinated Universal Time keeps in close agreement, within 0.9 seconds, with Universal Time.

### 3.1.2. Coordinate

In order to analyze satellite operation, many different bodies must be simulated. This involves multiple coordinates, which must be well defined for optimal analysis. Inertial reference frame and body fixed frames are used together for calculating various orbit dynamics.

For calculating orbit dynamics, it is important that all acting forces are integrated in the same reference frame. In this study, the reference is set to Earth Centered Inertial (ECI) reference frame, where X-axis points to the vernal equinox and Z-axis points to the North Pole. Note that the Earth Centered Inertial reference frame is quasi-inertial, since it does not include secular change of Earth's rotation axis and the equinox known as precession, and periodic and short-term change of the equator and the equinox. If higher precision is required, precession and nutation must be considered into the Earth's relative motion.

Earth fixed coordinates are used for calculating geopotential force acting on the satellite and for retrieving satellite passes. The coordinate is given in spherical coordinates $(r, \lambda, \varphi)$ with x axis pointing the Greenwich meridian, z axis pointing the North Pole where $r$ represents the radial distance, $\lambda$ represents the geocentric longitude, and $\varphi$ represents the geocentric latitude. The parameters can be obtained from the following set of equations:

$$r = \sqrt{x^2 + y^2 + z^2}, \tag{3.6}$$

$$\lambda = \tan^{-1}\frac{y}{x} - \theta, \tag{3.7}$$

$$\varphi = \vartheta - \frac{\pi}{2} = \sin^{-1}\frac{z}{r}, \tag{3.8}$$

Where $x, y, z$ are the inertial coordinates of the satellite and θ represents the Greenwich apparent sidereal time (GAST). GAST can be calculated using the equation

$$\theta = \theta_m + \Delta\psi \cos\varepsilon, \tag{3.9}$$

where $\theta_m$ is the Greenwich Mean Sidereal Time, $\Delta\psi$ is the periodic shift of the vernal equinox and $\varepsilon$ is the obliquity of the ecliptic. However, since this study neglects the effect of precession and nutation, $\Delta\psi \cos\varepsilon = 0$, and thus $\theta = \theta_m$.

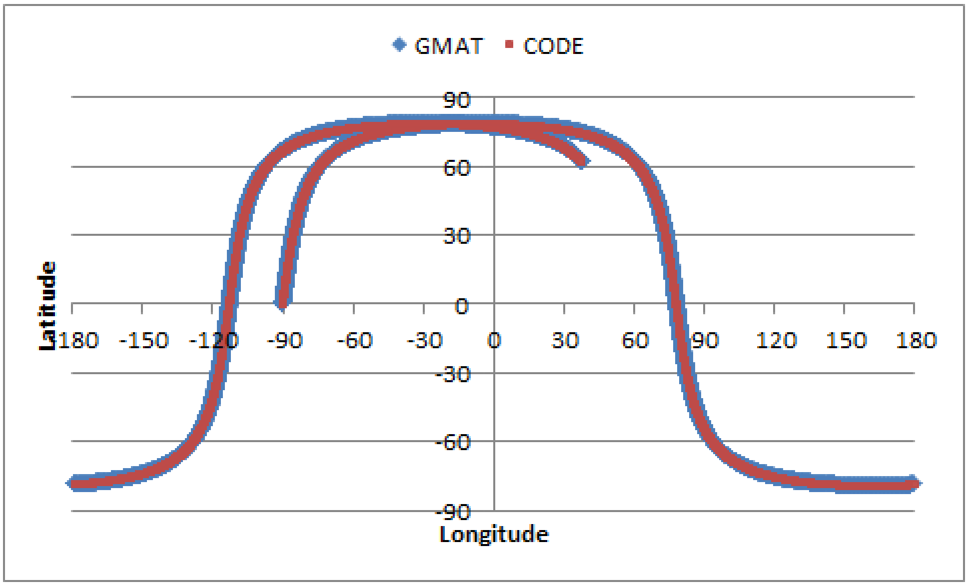


**Figure 4** Longitude and latitude plot compared with GMAT

### 3.1.3. Initialization

In order to initialize the states for the numerical analysis, this study takes orbital elements as the input. When the orbital elements semimajor axis $a$, eccentricity $e$, inclination $i$, right ascension of the ascending node $\Omega$, argument of periapsis $\omega$, and true anomaly $\nu$ are given, the inertial states $R_i$ and $V_i$ are obtained by

$$R_i = AR_p, \tag{3.10}$$
$$V_i = AV_p, \tag{3.11}$$

where

$$R_p = \begin{bmatrix} \frac{a(1-e^2)}{1+e\cos\nu}\cos\nu \\ \frac{a(1-e^2)}{1+e\cos\nu}\sin\nu \\ 0 \end{bmatrix}, \tag{3.12}$$
$$V_p = \sqrt{\frac{\mu}{a(1-e^2)}}\begin{bmatrix} -\sin\nu \\ e+\cos\nu \\ 0 \end{bmatrix}, \tag{3.13}$$
$$A = \begin{bmatrix} cos\,\Omega\cos\omega - \sin\Omega\sin\omega\cos i & -\cos\Omega\sin\omega - \sin\Omega\cos\omega\cos i & \sin\Omega\sin i \\ \sin\Omega\cos\omega + \cos\Omega\sin\omega\cos i & -\sin\Omega\sin\omega + \cos\Omega\cos\omega\cos i & -\cos\Omega\sin i \\ \sin\omega\sin i & \cos\omega\sin i & \cos i \end{bmatrix}. \tag{3.14}$$

## 3.2. Ephemerides

Ephemerides give the positions of the planets, which are required for third body perturbation and solar radiation pressure in numerical analysis. This study adopts van Flandern et al.'s method [1979] of calculating the ephemerides. Van Flandern et al.'s method is favorable in this study because it only requires a single parameter while his method provides a one arcminute precision, which is adequate for the purpose of this study.

Van Flandern et al. defines $t$ and $T$ as

$$t = \mathrm{JD} - 2451545.0, \tag{3.15}$$
$$T = t/36525 + 1, \tag{3.16}$$

where JD is a given Julian date and fraction.

Then, the fundamental arguments for calculating the ephemerides are given as

| | | |
|---|---|---|
| Moon | (1) $L_M = 0.606434 + 0.03660110129t,$ | (3.17) |
| | (2) $G_M = 0.374897 + 0.03629164709t,$ | (3.18) |
| | (3) $F_M = 0.259091 + 0.03674819520t,$ | (3.19) |
| | (4) $\mathrm{D} = L_M - L_S = 0.827362 + 0.03386319198t,$ | (3.20) |
| | (5) $\Omega_M = L_M - F_M = 0.347343 - 0.00014709391t,$ | (3.21) |
| Sun | (7) $L_S = 0.779072 + 0.00273790931t,$ | (3.22) |
| | (8) $G_S = 0.993126 + 0.00273777850t,$ | (3.23) |
| Mercury | (9) $L_1 = 0.700695 + 0.01136771400t,$ | (3.24) |
| | (10) $G_1 = 0.485541 + 0.01136759566t,$ | (3.25) |
| | (11) $F_1 = 0.566441 + 0.01136762384t,$ | (3.26) |
| Venus | (12) $L_2 = 0.505498 + 0.00445046867t,$ | (3.27) |
| | (13) $G_2 = 0.140023 + 0.00445036173t,$ | (3.28) |
| | (14) $F_2 = 0.292498 + 0.00445040017t,$ | (3.29) |
| Mars | (15) $L_4 = 0.987353 + 0.00145575328t,$ | (3.30) |
| | (16) $G_4 = 0.053856 + 0.00145561327t,$ | (3.31) |
| | (17) $F_4 = 0.849694 + 0.00145569465t,$ | (3.32) |
| Jupiter | (18) $L_5 = 0.089608 + 0.00023080893t,$ | (3.33) |
| | (19) $G_5 = 0.056531 + 0.00023080893t,$ | (3.34) |
| | (20) $F_5 = 0.814794 + 0.00023080893t,$ | (3.35) |
| Saturn | (21) $L_6 = 0.133295 + 0.00009294371t,$ | (3.36) |
| | (22) $G_6 = 0.882987 + 0.00009294371t,$ | (3.37) |
| | (23) $F_6 = 0.821218 + 0.00009294371t,$ | (3.38) |
| Uranus | (24) $L_7 = 0.870169 + 0.00003269438t,$ | (3.39) |
| | (25) $G_7 = 0.400589 + 0.00003269438t,$ | (3.40) |
| | (26) $F_7 = 0.664614 + 0.00003265562t,$ | (3.41) |
| Neptune | (27) $L_8 = 0.846912 + 0.00001672092t,$ | (3.42) |
| | (28) $G_8 = 0.725368 + 0.00001672092t,$ | (3.43) |
| | (29) $F_8 = 0.480856 + 0.00001663715t,$ | (3.44) |
| Pluto | (31) $L_9 = 0.663854 + 0.00001115482t,$ | (3.45) |
| | (32) $G_9 = 0.041020 + 0.00001104864t,$ | (3.46) |
| | (33) $F_9 = 0.357355 + 0.00001104864t.$ | (3.47) |

The arguments are given in numbers of revolutions, and therefore when used in trigonometric arguments, they must be converted into radians. Using the arguments, heliocentric longitude and latitude, and the radius vectors can be calculated for the eight major planets and geocentric ecliptic coordinates of the Sun and the Moon can be calculated using polynomial functions.

The polynomial functions are given in the appendix as tables which look as in Table 3.

**Table 3** Example of van Flandern's polynomial functions

PLON

| | | | TRIGONOMETRIC ARGUMENTS | | | | | | | | |
|---|---|---|---|---|---|---|---|---|---|---|---|
| COEFFICIENT | $T$ | | 1 | 5 | 7 | 8 | 12 | 13 | 14 | 16 | 19 |
| 2814 | 0 | SIN | 0 | 0 | 0 | 0 | 0 | 1 | 0 | 0 | 0 |
| -181 | 0 | SIN | 0 | 0 | 0 | 0 | 0 | 0 | 2 | 0 | 0 |
| -20 | 1 | SIN | 0 | 0 | 0 | 0 | 0 | 1 | 0 | 0 | 0 |
| 12 | 0 | SIN | 0 | 0 | 0 | 0 | 0 | 2 | 0 | 0 | 0 |
| -10 | 0 | COS | 0 | 0 | 0 | 2 | 0 | -2 | 0 | 0 | 0 |
| 7 | 0 | COS | 0 | 0 | 0 | 3 | 0 | -3 | 0 | 0 | 0 |

The coefficients, $T$, and the trigonometric arguments in the table is read as,

$$\mathrm{PLON} = \lambda - \mathrm{L} = 2814 \sin G_2 - 181 \sin F_2 - 20T \sin G_2 + 12 \sin 2G_2 - 10 \cos(2G_S - 2G_2) + 7 \cos(3G_S - 3G_2). \quad (3.48)$$

The units of PLON and $\beta$ are given in arcseconds, RP given in astronomical units for planets and earth radii for the Moon. However, since the ephemerides are given in the ecliptic coordinates, they must be transformed into equatorial coordinates in order to be used in the study.

In order to obtain the ephemerides given in equatorial coordinates, the series for $U$, $V$, and $W$ must be further calculated, which are also given in the appendix. Then, the right ascension α, declination δ, and geocentric distance $\rho$ can be obtained by

$$\alpha = L + sin\left[\frac{W}{(U-V^2)^{1/2}}\right], \quad (3.49)$$

$$\delta = sin^{-1}\left(\frac{V}{\sqrt{U}}\right), \quad (3.50)$$

$$\rho = \bar{\Delta}\sqrt{U}, \quad (3.51)$$

where $L$ is given in the fundamental arguments for the corresponding planet and $\bar{\Delta}$ is the scaling factors as shown in table 4.

**Table 4** Scaling factor $\bar{\Delta}$ for corresponding planets

| | |
|---|---:|
| Mercury | 1.07693 |
| Venus | 1.23437 |
| Mars | 1.83094 |
| Jupiter | 5.30693 |
| Saturn | 9.61711 |
| Uranus | 19.24877 |
| Neptune | 30.08900 |
| Pluto | 41.32680 |
| Sun | 1.00021 |
| Moon | 60.40974 |

The results of van Flandern et al.'s method for the Moon and the Sun, which is used in this study is compared with the results from the HORIZONS system as in Table 5 and Table 6 show that the ephemerides do provide adequate accuracy for this study.

If higher precision for ephemerides is required, the use of HORIZONS system by Jet Propulsion Laboratory (JPL) Solar System Dynamics is recommended.

**Table 5** van Flandern error for the Moon compared to HORIZONS

| Julian Date | Luna R.A_apparent (HORIZONS) | Luna DEC_apparent (HORIZONS) | Luna RP (HORIZONS) | Luna R.A_apparent (Flandern) | Luna DEC_apparent (Flandern) | Luna RP (Flandern) | Luna R.A_apparent error | Luna DEC_apparent error | Luna RP error |
|---|---|---|---|---|---|---|---|---|---|
| 2456123.5 | 63.82931 | 21.11838 | 0.002699389 | 63.8193 | 21.1198 | 63.3228 | 0.01001 | -0.00142 | -58.43459894 |
| 2456124.5 | 76.68532 | 21.66502 | 0.00268723 | 76.6734 | 21.6664 | 63.0365 | 0.01192 | -0.00138 | -51.43417494 |
| 2456125.5 | 89.71729 | 21.21248 | 0.002670093 | 89.7036 | 21.2141 | 62.6326 | 0.01369 | -0.00162 | -38.94660517 |
| 2456126.5 | 102.78768 | 19.74626 | 0.002649464 | 102.773 | 19.7489 | 62.1464 | 0.01468 | -0.00264 | -23.95133559 |
| 2456127.5 | 115.76932 | 17.30957 | 0.00262679 | 115.754 | 17.3137 | 61.6122 | 0.01532 | -0.00413 | -8.728014836 |
| 2456128.5 | 128.58224 | 14.00291 | 0.002603339 | 128.567 | 14.0087 | 61.0601 | 0.01524 | -0.00579 | 4.36232184 |
| 2456129.5 | 141.21499 | 9.97522 | 0.002580098 | 141.2 | 9.98231 | 60.5134 | 0.01499 | -0.00709 | 14.61472714 |
| 2456130.5 | 153.72736 | 5.41182 | 0.002557743 | 153.713 | 5.41978 | 59.988 | 0.01436 | -0.00796 | 21.40811863 |
| 2456131.5 | 166.23951 | 0.5241 | 0.00253667 | 166.226 | 0.532527 | 59.4932 | 0.01351 | -0.008427 | 24.78882306 |
| 2456132.5 | 178.91379 | -4.45594 | 0.002517105 | 178.901 | -4.44755 | 59.0342 | 0.01279 | -0.00839 | 25.50529949 |
| 2456133.5 | 191.93162 | -9.27655 | 0.002499257 | 191.918 | -9.2689 | 58.6158 | 0.01362 | -0.00765 | 24.11563297 |
| 2456134.5 | 205.46267 | -13.6654 | 0.002483474 | 205.449 | -13.6594 | 58.2459 | 0.01367 | -0.006 | 22.24162897 |
| 2456135.5 | 219.62193 | -17.33389 | 0.002470359 | 219.607 | -17.3304 | 57.9385 | 0.01493 | -0.00349 | 20.94355989 |
| 2456136.5 | 234.41668 | -19.99583 | 0.002460807 | 234.402 | -19.995 | 57.7144 | 0.01468 | -0.00083 | 21.30741482 |
| 2456137.5 | 249.70253 | -21.40712 | 0.002455925 | 249.687 | -21.4084 | 57.5998 | 0.01553 | 0.00128 | 21.94005006 |
| 2456138.5 | 265.18592 | -21.42093 | 0.002456849 | 265.17 | -21.4235 | 57.6213 | 0.01592 | 0.00257 | 22.98874483 |
| 2456139.5 | 280.49805 | -20.03379 | 0.002464479 | 280.482 | -20.0369 | 57.8001 | 0.01605 | 0.00311 | 24.02488184 |
| 2456140.5 | 295.31203 | -17.39331 | 0.002479212 | 295.296 | -17.3968 | 58.1458 | 0.01603 | 0.00349 | 23.08837541 |
| 2456141.5 | 309.43387 | -13.76018 | 0.002500737 | 309.419 | -13.7642 | 58.6511 | 0.01487 | 0.00402 | 20.34590334 |
| 2456142.5 | 322.82376 | -9.44688 | 0.002527968 | 322.811 | -9.45179 | 59.2908 | 0.01276 | 0.00491 | 13.94633027 |
| 2456143.5 | 335.56197 | -4.76275 | 0.002559122 | 335.55 | -4.76859 | 60.0232 | 0.01197 | 0.00584 | 3.215007483 |
| 2456144.5 | 347.7982 | 0.01883 | 0.002591927 | 347.786 | 0.0122906 | 60.7947 | 0.0122 | 0.0065394 | -9.960663986 |
| 2456145.5 | 359.70964 | 4.67142 | 0.002623893 | 359.697 | 4.66477 | 61.5468 | 0.01264 | 0.00665 | -25.03842205 |
| 2456146.5 | 11.47368 | 9.012 | 0.002652588 | 11.4597 | 9.00609 | 62.2218 | 0.01398 | 0.00591 | -37.5647873 |
| 2456147.5 | 23.25116 | 12.89062 | 0.002675882 | 23.2367 | 12.8864 | 62.7697 | 0.01446 | 0.00422 | -47.37315852 |
| 2456148.5 | 35.17436 | 16.17919 | 0.002692123 | 35.1601 | 16.1773 | 63.1515 | 0.01426 | 0.00189 | -52.86879366 |
| 2456149.5 | 47.33618 | 18.76309 | 0.002700253 | 47.3228 | 18.7636 | 63.3425 | 0.01338 | -0.00051 | -54.87883935 |
| 2456150.5 | 59.78012 | 20.53803 | 0.002699863 | 59.7677 | 20.5406 | 63.3333 | 0.01242 | -0.00257 | -54.50098728 |
| 2456151.5 | 72.49437 | 21.41331 | 0.002691203 | 72.4826 | 21.4171 | 63.1296 | 0.01177 | -0.00379 | -50.80931763 |
| 2456152.5 | 85.41512 | 21.32077 | 0.002675141 | 85.4034 | 21.325 | 62.7519 | 0.01172 | -0.00423 | -44.68441018 |
| 2456153.5 | 98.4434 | 20.22695 | 0.002653081 | 98.431 | 20.231 | 62.2332 | 0.0124 | -0.00405 | -36.47447864 |
| | | | | | | | | | |
| 2456123.5 | 63.82931 | 21.11838 | 0.002699389 | 63.8193 | 21.1198 | 63.3228 | 0.01001 | -0.00142 | -58.43459894 |
| 2456488.5 | 186.89787 | -6.17435 | 0.002578625 | 186.882 | -6.16668 | 60.4747 | 0.01587 | -0.00767 | 41.00106784 |
| 2456853.5 | 329.04913 | -8.16361 | 0.002410835 | 329.031 | -8.17071 | 56.5486 | 0.01813 | 0.0071 | -18.84174275 |
| 2457218.5 | 100.11883 | 18.08937 | 0.002600623 | 100.104 | 18.0936 | 60.997 | 0.01483 | -0.00423 | 0.584891931 |
| 2457584.5 | 234.21911 | -14.38729 | 0.002689962 | 234.206 | -14.3873 | 63.0893 | 0.01311 | 1E-05 | 20.46811333 |
| 2457949.5 | 1.27567 | -2.76045 | 0.002562681 | 1.26489 | -2.76629 | 60.1166 | 0.01078 | 0.00584 | -60.18092079 |
| 2458314.5 | 141.97844 | 16.23009 | 0.002406552 | 141.964 | 16.2342 | 56.4469 | 0.01444 | -0.00411 | -10.924758 |
| 2458679.5 | 270.52059 | -21.87098 | 0.002627709 | 270.501 | -21.8694 | 61.6304 | 0.01959 | -0.00158 | 12.64487423 |
| 2459045.5 | 43.7848 | 12.90467 | 0.002681496 | 43.7724 | 12.9027 | 62.9022 | 0.0124 | 0.00197 | -52.55816947 |
| 2459410.5 | 174.4955 | 7.87757 | 0.00254537 | 174.481 | 7.8827 | 59.697 | 0.0145 | -0.00513 | 26.40340341 |
| 2459775.5 | 313.86207 | -22.53826 | 0.002404933 | 313.847 | -22.5397 | 56.4105 | 0.01507 | 0.00144 | -20.93743296 |
| 2460140.5 | 80.09055 | 27.01009 | 0.002654254 | 80.0779 | 27.0078 | 62.2561 | 0.01265 | 0.00229 | -7.032146117 |
| 2460506.5 | 211.56894 | -15.02989 | 0.002673766 | 211.558 | -15.0268 | 62.7072 | 0.01094 | -0.00309 | 34.76416468 |
| 2460871.5 | 345.17253 | -6.91806 | 0.002520247 | 345.16 | -6.92488 | 59.1193 | 0.01253 | 0.00682 | -47.19868781 |
| 2461236.5 | 123.68918 | 22.44343 | 0.002417183 | 123.672 | 22.4507 | 56.6966 | 0.01718 | -0.00727 | -13.06786463 |
| 2461601.5 | 249.85753 | -26.72263 | 0.002670934 | 249.842 | -26.719 | 62.6461 | 0.01553 | -0.00363 | 0.779296571 |
| 2461967.5 | 20.66383 | 14.39308 | 0.002669331 | 20.6511 | 14.3896 | 62.617 | 0.01273 | 0.00348 | -53.48339815 |
| 2462332.5 | 155.43287 | 5.30503 | 0.002493635 | 155.418 | 5.31189 | 58.4833 | 0.01487 | -0.00686 | 28.06507023 |
| 2462697.5 | 292.5619 | -18.76826 | 0.002435042 | 292.544 | -18.7682 | 57.1136 | 0.0179 | -6E-05 | -1.16396538 |
| 2463062.5 | 60.5636 | 20.1597 | 0.002683789 | 60.5548 | 20.1614 | 62.9518 | 0.0088 | -0.0017 | -25.88787184 |
| 2463428.5 | 192.49179 | -7.39763 | 0.002664782 | 192.476 | -7.39063 | 62.494 | 0.01579 | -0.007 | 50.59654437 |
| 2463793.5 | 328.18374 | -8.85623 | 0.002463623 | 328.171 | -8.86325 | 57.7883 | 0.01274 | 0.00702 | -28.86901845 |
| 2464158.5 | 103.04244 | 18.01867 | 0.002461893 | 103.023 | 18.0245 | 57.7434 | 0.01944 | -0.00583 | -1.290214207 |
| 2464523.5 | 231.66049 | -13.61584 | 0.002691025 | 231.652 | -13.6143 | 63.1154 | 0.00849 | -0.00154 | 13.07155763 |
| 2464889.5 | 5.68419 | -1.75071 | 0.002657682 | 5.67325 | -1.75552 | 62.3449 | 0.01094 | 0.00481 | -60.60049471 |
| 2465254.5 | 141.49516 | 16.97206 | 0.002437654 | 141.485 | 16.9799 | 57.1743 | 0.01016 | -0.00784 | 2.503550619 |
| 2465619.5 | 273.75185 | -22.75002 | 0.002492063 | 273.73 | -22.7466 | 58.4474 | 0.02185 | -0.00342 | 21.89946188 |
| 2465984.5 | 41.56582 | 12.6086 | 0.002693558 | 41.5555 | 12.6023 | 63.1829 | 0.01032 | 0.0063 | -38.45591111 |
| 2466350.5 | 177.42158 | 6.26086 | 0.002650657 | 177.408 | 6.26545 | 62.1646 | 0.01358 | -0.00459 | 38.40549085 |
| 2466715.5 | 313.72406 | -22.62016 | 0.002411524 | 313.712 | -22.6227 | 56.5658 | 0.01206 | 0.00254 | -25.47226367 |
| 2467080.5 | 83.94571 | 27.75355 | 0.002526151 | 83.9262 | 27.7534 | 59.2508 | 0.01951 | 0.00015 | -2.706513002 |
| 2467445.5 | 209.51439 | -14.77687 | 0.002695272 | 209.505 | -14.7691 | 63.2136 | 0.00939 | -0.00777 | 22.15089512 |

**Table 6** van Flandern error for the Sun compared to HORIZONS

| Julian Date | Sol R.A_apparent (HORIZONS) | Sol DEC_apparent (HORIZONS) | Sol RP (HORIZONS) | Sol R.A_apparent (Flandern) | Sol DEC_apparent (Flandern) | Sol RP (Flandern) | Sol R.A_apparent error | Sol DEC_apparent error | Sol RP error |
|---|---|---|---|---|---|---|---|---|---|
| 2456123.5 | 114.74164 | 21.48943 | 1.016476047 | 114.741 | 21.488 | 1.0165 | 0.00064 | 0.00143 | -3583.351145 |
| 2456124.5 | 115.75171 | 21.32753 | 1.016428988 | 115.752 | 21.3262 | 1.01645 | -0.00029 | 0.00133 | -3143.35271 |
| 2456125.5 | 116.75966 | 21.15958 | 1.016376203 | 116.759 | 21.1583 | 1.01639 | 0.00066 | 0.00128 | -2064.054165 |
| 2456126.5 | 117.76544 | 20.98566 | 1.016317565 | 117.765 | 20.9845 | 1.01633 | 0.00044 | 0.00116 | -1860.316919 |
| 2456127.5 | 118.76897 | 20.80584 | 1.016252984 | 118.769 | 20.8047 | 1.01627 | -3E-05 | 0.00114 | -2545.514372 |
| 2456128.5 | 119.77021 | 20.62017 | 1.016182418 | 119.77 | 20.6192 | 1.0162 | 0.00021 | 0.00097 | -2630.218834 |
| 2456129.5 | 120.76909 | 20.42874 | 1.016105876 | 120.769 | 20.4278 | 1.01612 | 9E-05 | 0.00094 | -2112.868491 |
| 2456130.5 | 121.76556 | 20.23161 | 1.016023431 | 121.765 | 20.2307 | 1.01604 | 0.00056 | 0.00091 | -2478.71592 |
| 2456131.5 | 122.75957 | 20.02886 | 1.015935218 | 122.759 | 20.028 | 1.01596 | 0.00057 | 0.00086 | -3707.262028 |
| 2456132.5 | 123.75109 | 19.82055 | 1.015841442 | 123.751 | 19.8198 | 1.01587 | 9E-05 | 0.00075 | -4272.237937 |
| 2456133.5 | 124.74008 | 19.60677 | 1.015742365 | 124.74 | 19.606 | 1.01578 | 8E-05 | 0.00077 | -5630.18743 |
| 2456134.5 | 125.72653 | 19.38758 | 1.015638302 | 125.727 | 19.3868 | 1.01568 | -0.00047 | 0.00078 | -6237.879149 |
| 2456135.5 | 126.71041 | 19.16306 | 1.01552961 | 126.71 | 19.1623 | 1.01558 | 0.00041 | 0.00076 | -7538.220646 |
| 2456136.5 | 127.69171 | 18.93329 | 1.015416664 | 127.692 | 18.9325 | 1.01547 | -0.00029 | 0.00079 | -7978.997533 |
| 2456137.5 | 128.67043 | 18.69835 | 1.015299838 | 128.671 | 18.6975 | 1.01536 | -0.00057 | 0.00085 | -9000.039395 |
| 2456138.5 | 129.64655 | 18.45831 | 1.015179485 | 129.647 | 18.4573 | 1.01524 | -0.00045 | 0.00101 | -9052.977475 |
| 2456139.5 | 130.62009 | 18.21325 | 1.015055902 | 130.62 | 18.2122 | 1.01513 | 9E-05 | 0.00105 | -11084.86056 |
| 2456140.5 | 131.59104 | 17.96325 | 1.01492932 | 131.591 | 17.9621 | 1.015 | 4E-05 | 0.00115 | -10573.53278 |
| 2456141.5 | 132.55942 | 17.70838 | 1.014799882 | 132.56 | 17.7071 | 1.01487 | -0.00058 | 0.00128 | -10489.49745 |
| 2456142.5 | 133.52526 | 17.4487 | 1.014667642 | 133.525 | 17.4473 | 1.01474 | 0.00026 | 0.0014 | -10824.59138 |
| 2456143.5 | 134.48858 | 17.1843 | 1.014532573 | 134.489 | 17.1828 | 1.0146 | -0.00042 | 0.0015 | -10086.91662 |
| 2456144.5 | 135.44941 | 16.91525 | 1.014394581 | 135.45 | 16.9136 | 1.01446 | -0.00059 | 0.00165 | -9786.558314 |
| 2456145.5 | 136.40779 | 16.64163 | 1.014253522 | 136.408 | 16.6399 | 1.01432 | -0.00021 | 0.00173 | -9944.897257 |
| 2456146.5 | 137.36375 | 16.36351 | 1.014109224 | 137.364 | 16.3617 | 1.01417 | -0.00025 | 0.00181 | -9091.942348 |
| 2456147.5 | 138.31732 | 16.08098 | 1.013961496 | 138.318 | 16.0792 | 1.01401 | -0.00068 | 0.00178 | -7256.114396 |
| 2456148.5 | 139.26853 | 15.79412 | 1.013810142 | 139.269 | 15.7923 | 1.01386 | -0.00047 | 0.00182 | -7458.700927 |
| 2456149.5 | 140.21741 | 15.50301 | 1.013654966 | 140.218 | 15.5013 | 1.01369 | -0.00059 | 0.00171 | -5241.084892 |
| 2456150.5 | 141.16398 | 15.20775 | 1.013495775 | 141.165 | 15.2061 | 1.01353 | -0.00102 | 0.00165 | -5120.030906 |
| 2456151.5 | 142.10828 | 14.90842 | 1.013332381 | 142.109 | 14.9068 | 1.01336 | -0.00072 | 0.00162 | -4131.671055 |
| 2456152.5 | 143.05032 | 14.60511 | 1.013164605 | 143.051 | 14.6036 | 1.01319 | -0.00068 | 0.00151 | -3799.101701 |
| 2456153.5 | 143.99014 | 14.29791 | 1.012992272 | 143.991 | 14.2962 | 1.01301 | -0.00086 | 0.00171 | -2652.072175 |
| | | | | | | | | | |
| 2456123.5 | 114.74164 | 21.48943 | 1.016476047 | 114.741 | 21.488 | 1.0165 | 0.00064 | 0.00143 | -3583.351145 |
| 2456488.5 | 114.4961 | 21.52704 | 1.01644857 | 114.499 | 21.5258 | 1.01651 | -0.0029 | 0.00124 | -9189.798531 |
| 2456853.5 | 114.25219 | 21.56448 | 1.016427958 | 114.253 | 21.5634 | 1.01652 | -0.00081 | 0.00108 | -13769.32718 |
| 2457218.5 | 114.00441 | 21.60189 | 1.016516295 | 114.004 | 21.6008 | 1.01654 | 0.00041 | 0.00109 | -3546.187578 |
| 2457584.5 | 114.76831 | 21.48384 | 1.01644918 | 114.771 | 21.4822 | 1.0165 | -0.00269 | 0.00164 | -7602.576284 |
| 2457949.5 | 114.52169 | 21.5223 | 1.016444072 | 114.523 | 21.5207 | 1.01651 | -0.00131 | 0.0016 | -9862.666476 |
| 2458314.5 | 114.28034 | 21.56029 | 1.016501482 | 114.28 | 21.559 | 1.01653 | 0.00034 | 0.00129 | -4266.198911 |
| 2458679.5 | 114.03825 | 21.59796 | 1.016491285 | 114.036 | 21.5971 | 1.01654 | 0.00225 | 0.00086 | -7287.699216 |
| 2459045.5 | 114.80098 | 21.48031 | 1.016487135 | 114.799 | 21.4788 | 1.0165 | 0.00198 | 0.00151 | -1924.599354 |
| 2459410.5 | 114.55909 | 21.51924 | 1.01648603 | 114.559 | 21.5177 | 1.01652 | 9E-05 | 0.00154 | -5081.889262 |
| 2459775.5 | 114.32051 | 21.5565 | 1.016455757 | 114.317 | 21.5561 | 1.01653 | 0.00351 | 0.0004 | -11106.6625 |
| 2460140.5 | 114.07532 | 21.5948 | 1.016528132 | 114.07 | 21.5939 | 1.01654 | 0.00532 | 0.0009 | -1775.431072 |
| 2460506.5 | 114.84266 | 21.47554 | 1.016446819 | 114.841 | 21.4748 | 1.0165 | 0.00166 | 0.00074 | -7955.828907 |
| 2460871.5 | 114.59705 | 21.51398 | 1.016402711 | 114.597 | 21.5128 | 1.01652 | 5E-05 | 0.00118 | -17546.25 |
| 2461236.5 | 114.35471 | 21.55143 | 1.016463787 | 114.354 | 21.5501 | 1.01653 | 0.00071 | 0.00133 | -9905.28644 |
| 2461601.5 | 114.11244 | 21.58781 | 1.01646559 | 114.112 | 21.5868 | 1.01654 | 0.00044 | 0.00101 | -11131.64953 |
| 2461967.5 | 114.87353 | 21.46903 | 1.016457298 | 114.875 | 21.4665 | 1.01651 | -0.00147 | 0.00253 | -7884.131017 |
| 2462332.5 | 114.63126 | 21.50591 | 1.016487504 | 114.634 | 21.5038 | 1.01652 | -0.00274 | 0.00211 | -4861.337419 |
| 2462697.5 | 114.39257 | 21.54233 | 1.016456197 | 114.392 | 21.5408 | 1.01653 | 0.00057 | 0.00153 | -11040.71351 |
| 2463062.5 | 114.145 | 21.57959 | 1.016534209 | 114.142 | 21.5777 | 1.01654 | 0.003 | 0.00189 | -866.2860523 |
| 2463428.5 | 114.91159 | 21.45951 | 1.016484193 | 114.912 | 21.4578 | 1.01651 | -0.00041 | 0.00171 | -3860.737886 |
| 2463793.5 | 114.66562 | 21.49785 | 1.016436688 | 114.666 | 21.4961 | 1.01652 | -0.00038 | 0.00175 | -12463.34108 |
| 2464158.5 | 114.42184 | 21.53535 | 1.01650459 | 114.42 | 21.5344 | 1.01653 | 0.00184 | 0.00095 | -3801.283387 |
| 2464523.5 | 114.17955 | 21.57297 | 1.016495676 | 114.177 | 21.5727 | 1.01654 | 0.00255 | 0.00027 | -6630.822703 |
| 2464889.5 | 114.93768 | 21.45481 | 1.016437314 | 114.937 | 21.4538 | 1.01651 | 0.00068 | 0.00101 | -10873.62269 |
| 2465254.5 | 114.69254 | 21.49418 | 1.016462523 | 114.694 | 21.493 | 1.01652 | -0.00146 | 0.00118 | -8598.462302 |
| 2465619.5 | 114.45199 | 21.53236 | 1.016422566 | 114.452 | 21.5319 | 1.01653 | -1E-05 | 0.00046 | -16071.82928 |
| 2465984.5 | 114.20275 | 21.57152 | 1.016496073 | 114.201 | 21.5702 | 1.01655 | 0.00175 | 0.00132 | -8067.413157 |
| 2466350.5 | 114.97003 | 21.4526 | 1.016476156 | 114.971 | 21.4508 | 1.01651 | -0.00097 | 0.0018 | -5062.984175 |
| 2466715.5 | 114.72736 | 21.49091 | 1.016420975 | 114.728 | 21.4894 | 1.01652 | -0.00064 | 0.00151 | -14813.95294 |
| 2467080.5 | 114.48518 | 21.52934 | 1.016495545 | 114.484 | 21.5274 | 1.01654 | 0.00118 | 0.00194 | -6650.402871 |
| 2467445.5 | 114.24657 | 21.56606 | 1.016509147 | 114.245 | 21.5648 | 1.01655 | 0.00157 | 0.00126 | -6111.516055 |

## 3.3. Rotation Elements

Although ephemerides can be obtained from van Flandern et al.'s method, his method does not provide pole information of the planets. Therefore, in order to simulate orbits around other planets, additional information of the poles is required.

The IAU/IAG working group performs such work and updates the rotation axis and prime meridian of planets every three years [Seidelman et al., 2007]. The poles and prime meridian are given in the International Celestial Reference Frame (ICRF), which has a small rotation smaller than 0.1 arcsecond with the mean dynamic frame of J2000.0. The right ascension $\alpha_0$, declination $\delta_0$, and the angle between the intersection of equator of ICRF and equator of the planet with the prime meridian $W_0$. The reference system for defining the orientation is shown as in Figure 5 [Seidelman et al., 2007, p. 158].

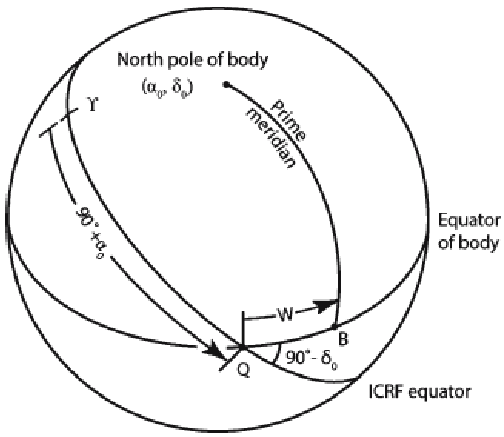


**Figure 5** Reference systems for calculating the rotation elements

The rotation elements can be obtained from polynomials given, which are similar in form as in van Flandern's method. As an example for Earth and the Moon, the equations are given as

$$t = \mathrm{JD} - 2451545.0, \tag{3.51}$$
$$T_0 = t/36525, \tag{3.52}$$

with

$$\alpha_{0,Earth} = 0.00 - 0.641T, \tag{3.52}$$
$$\delta_{0,Earth} = 90.00 - 0.557T, \tag{3.53}$$
$$W_{0,Earth} = 190.147 + 360.9856235d, \tag{3.54}$$

for Earth and

$$\alpha_{0,Moon} = 269.9949 + 0.0031T - 3.8787\sin E1 - 0.1204\sin E2 + 0.0700\sin E3 - 0.0172\sin E4 + 0.0072\sin E6 - 0.0052\sin E10 + 0.0043\sin E13, \tag{3.55}$$

$$\delta_{0,Moon} = 66.5392 + 0.0130T + 1.5419\cos E1 + 0.0239\cos E2 - 0.0278\cos E3 + 0.0068\cos E4 - 0.0029\cos E6 + 0.0009\cos E7 + 0.0008\cos E10 - 0.0009\cos E13, \tag{3.56}$$

$$W_{0,Moon} = 38.3213 + 13.17635815d - 1.4\times 10^{-12}d^2 + 3.5610\sin E1 + 0.1208\sin E2 - 0.0642\sin E3 + 0.0158\sin E4 + 0.0252\sin E5 - 0.0066\sin E6 - 0.0047\sin E7 - 0.0046\sin E8 + 0.0028\sin E9 + 0.0052\sin E10 + 0.0040\sin E11 + 0.0019\sin E12 - 0.0044\sin E13, \tag{3.57}$$

for Moon with

$$E1 = 125.045 - 0.0529921d, \tag{3.58}$$
$$E2 = 250.089 - 0.1059842d, \tag{3.59}$$
$$E3 = 260.008 + 13.0120009d, \tag{3.60}$$
$$E4 = 176.625 + 13.3407154d, \tag{3.61}$$
$$E5 = 357.529 + 0.9856003d, \tag{3.62}$$
$$E6 = 311.589 + 26.4057084d, \tag{3.63}$$
$$E7 = 134.963 + 13.0649930d, \tag{3.64}$$
$$E8 = 276.617 + 0.3287146d, \tag{3.65}$$
$$E9 = 34.226 + 1.7484877d, \tag{3.66}$$
$$E10 = 15.134 - 0.1589763d, \tag{3.67}$$
$$E11 = 119.743 + 0.0036096d, \tag{3.68}$$
$$E12 = 239.961 + 0.1643573d, \tag{3.69}$$
$$E13 = 25.053 + 12.9590088d. \tag{3.70}$$

**Table 7** Results of rotation element compared to HORIZONS

| Julian Date | IAU/IAG | | HORIZONS | | Error | |
|---|---|---|---|---|---|---|
| | N.Pole-RA | N.Pole-DC | N.Pole-RA | N.Pole-DC | N.Pole-RA | N.Pole-DC |
| 2456163.5 | 273.214745 | 65.7801163 | 273.21474 | 65.78011 | 0.0000051 | 0.0000063 |
| 2456164.5 | 273.205491 | 65.7736831 | 273.20548 | 65.77368 | 0.0000107 | 0.0000031 |
| 2456165.5 | 273.200019 | 65.7666438 | 273.20002 | 65.76664 | -0.0000011 | 0.0000038 |
| 2456166.5 | 273.198547 | 65.7595025 | 273.19855 | 65.7595 | -0.0000031 | 0.0000025 |
| 2456167.5 | 273.200855 | 65.7527530 | 273.20086 | 65.75275 | -0.0000046 | 0.0000030 |
| 2456168.5 | 273.206341 | 65.7468137 | 273.20635 | 65.74681 | -0.0000093 | 0.0000037 |
| 2456169.5 | 273.214128 | 65.7419777 | 273.21413 | 65.74197 | -0.0000025 | 0.0000077 |
| 2456170.5 | 273.223217 | 65.7383867 | 273.22322 | 65.73838 | -0.0000027 | 0.0000067 |
| 2456171.5 | 273.232646 | 65.7360326 | 273.23265 | 65.73603 | -0.0000043 | 0.0000026 |
| 2456172.5 | 273.241617 | 65.7347851 | 273.24162 | 65.73478 | -0.0000035 | 0.0000051 |
| 2456173.5 | 273.249589 | 65.7344375 | 273.24959 | 65.73444 | -0.0000015 | -0.0000025 |
| 2456174.5 | 273.256302 | 65.7347607 | 273.25631 | 65.73476 | -0.0000085 | 0.0000007 |
| 2456175.5 | 273.261740 | 65.7355540 | 273.26174 | 65.73555 | -0.0000003 | 0.0000040 |
| 2456176.5 | 273.266045 | 65.7366810 | 273.26605 | 65.73668 | -0.0000048 | 0.0000010 |
| 2456177.5 | 273.269403 | 65.738084 | 273.26941 | 65.73809 | -0.0000067 | -0.0000060 |
| 2456178.5 | 273.271930 | 65.7397746 | 273.27193 | 65.73978 | -0.0000001 | -0.0000054 |
| 2456179.5 | 273.273585 | 65.7418034 | 273.27359 | 65.74181 | -0.0000050 | -0.0000066 |
| 2456180.5 | 273.274137 | 65.7442164 | 273.27414 | 65.74422 | -0.0000028 | -0.0000036 |
| 2456181.5 | 273.273185 | 65.7470093 | 273.27318 | 65.74701 | 0.0000051 | -0.0000007 |
| 2456182.5 | 273.270236 | 65.7500907 | 273.27023 | 65.75009 | 0.0000060 | 0.0000007 |
| 2456183.5 | 273.264823 | 65.7532636 | 273.26482 | 65.75327 | 0.0000029 | -0.0000065 |
| 2456184.5 | 273.256636 | 65.7562315 | 273.25663 | 65.75623 | 0.0000062 | 0.0000015 |
| 2456185.5 | 273.245641 | 65.7586295 | 273.24563 | 65.75863 | 0.0000110 | -0.0000005 |
| 2456186.5 | 273.232151 | 65.7600747 | 273.23214 | 65.76008 | 0.0000114 | -0.0000053 |
| 2456187.5 | 273.216845 | 65.7602278 | 273.21683 | 65.76023 | 0.0000151 | -0.0000022 |
| 2456188.5 | 273.200709 | 65.7588531 | 273.2007 | 65.75885 | 0.0000090 | 0.0000031 |
| 2456189.5 | 273.184925 | 65.7558656 | 273.18491 | 65.75586 | 0.0000146 | 0.0000056 |
| 2456190.5 | 273.170711 | 65.7513548 | 273.1707 | 65.75135 | 0.0000114 | 0.0000048 |
| 2456191.5 | 273.159157 | 65.7455805 | 273.15915 | 65.74558 | 0.0000065 | 0.0000005 |
| 2456192.5 | 273.151063 | 65.7389406 | 273.15106 | 65.73894 | 0.0000026 | 0.0000006 |
| 2456193.5 | 273.146841 | 65.7319161 | 273.14684 | 65.73191 | 0.0000012 | 0.0000061 |

The results of rotation element calculation for selected Julian dates are compared with the HORIZONS system, which are shown in Table 7.

## 3.4. Shadow

Shadow, or the eclipse, is required for both solar radiation pressure in the equation of motion and for analyzing solar power generation of the solar panels. The determination of eclipse is performed using basic geometry.

The effect of the atmosphere or oblateness of the Earth is neglected and only geometry is considered. According to Montenbruck et al. [2000, p. 80], a fundamental plane $s_0$ is placed in the opposite direction of the Sun vector so that it is perpendicular to the shadow axis and intersects the satellite as

$$s_0 = (-\vec{s}^T \vec{s}_\odot)/|\vec{s}_\odot|, \tag{3.71}$$

where $\vec{s} = \vec{r} - \vec{r}_B$ is the spacecraft vector and $\vec{s}_\odot = \vec{r}_\odot - \vec{r}_B$ is the Sun vector relative to the occulting body at $\vec{r}_B$. From geometry, the distance between the spacecraft and the shadow axis, $l$ is given as

$$l = \sqrt{|\vec{s}|^2 + s_0^2}. \tag{3.72}$$

If two intersecting points for the solar ray $V_1$ and $V_2$ are set, and the distance from the intersecting points to the fundamental plane $c_1$ and $c_1$ are defined as

$$c_1 = s_0 + R_B/\sin f_1, \tag{3.73}$$
$$c_2 = s_0 - R_B/\sin f_2, \tag{3.74}$$

where $R_B$ is the radius of the occulting body, and $f_1$ and $f_2$ are the angles of the shadow cone of the penumbra, partial eclipse region, and the umbra, total eclipse region, respectively given as

$$sin\, f_1 = (R_\odot + R_B)/s_\odot, \tag{3.75}$$
$$sin\, f_2 = (R_\odot - R_B)/s_\odot, \tag{3.76}$$

where $R_\odot$ is the radius of the Sun, the radius for the penumbra shadow cone $l_1$ and the umbra shadow cone $l_2$ is given as

$$l_1 = c_1 \tan f_1, \quad (3.77)$$
$$l_2 = c_2 \tan f_2. \quad (3.78)$$

Analyzing the equations, if the satellite is located between the occulting body and $V_2$, $s_0 > 0$, $c_1 > 0$, $c_2 < 0$, and thus $l_1 > 0$, $l_2 < 0$. If the satellite is located between $V_1$ and the occulting body, $s_0 < 0$, $c_1 > 0$ unless $|s_0| > R_B/\sin f_1$, $c_2 < 0$, and thus $l_1 > 0$, $l_2 < 0$. Therefore if the satellite is between $V_1$ and $V_2$, the satellite is within the umbra region if $|l_2| > l$ and the satellite is within the penumbra region for $l_1 > l > |l_2|$ for $|l_2| < l_1$.

If $|l_2| \geq l_1$, satellite is in sunlight, and if the satellite is located beyond $V_2$, $l_2 > 0$ and thus the satellite is within the umbra region if $l_2 > l$ and the satellite is within the penumbra region for $l_1 > l > l_2$.

Since the umbra region is the total eclipse region, $E_\odot = 0$, and for full sunlight exposure, $E_\odot = 1$. However, when the satellite is within the penumbra region, further analysis must be performed for an approximate sunlight exposure. According to Montenbruck et al. [2000, p. 82], the occulted area of the Sun $A_\odot$ is given as

$$A_\odot = a^2 \cos^{-1}\frac{x}{a} + b^2 \cos^{-1}\frac{c-x}{b} - cy, \quad (3.79)$$
$$a = \sin^{-1}\frac{R_\odot}{|\vec{r}_\odot - \vec{r}|}, \quad (3.80)$$
$$b = \sin^{-1}\frac{R_B}{|\vec{s}|}, \quad (3.81)$$
$$c = \cos^{-1}\frac{-\vec{s}^T(\vec{r}_\odot - \vec{r})}{|\vec{s}||\vec{r}_\odot - \vec{r}|}, \quad (3.82)$$
$$x = \frac{c^2 + a^2 - b^2}{2c}, \quad (3.83)$$
$$y = \sqrt{a^2 - x^2}, \quad (3.84)$$

where $a$ is the apparent radius of the occulted body, $b$ is the apparent radius of the occulting body, and $c$ is the apparent separation of the centers of the bodies (in which the two bodies overlap for $c = 0$). Then, $E_\odot$ is given as

$$E_\odot = 1 - \frac{A_\odot}{\pi a^2}. \quad (3.85)$$

Note that $|a - b| < c < a + b$ must be satisfied for the occultation to take place, which automatically is satisfied if used only within the conditions $l_1 > l > |l_2|$.

## 3.5. Atmospheric model

The atmosphere model used in this study is Jacchia 77 model [Jacchia, 1977]. Jacchia 77 is the revised model of Jacchia 71. Jacchia presents a static model for atmospheric heights of 90 km and above and relations for calculating the exospheric temperature.

This study adopts the Jacchia 77 model realized using FORTRAN subroutine by David L. Huestis (SRI International). The U.S. Standard Atmosphere 1976 is applied for atmospheric altitude up to 86 km, and Jacchia 77 is applied for atmospheric altitude from 90 km. Polynomial fit connects the atmospheric altitude between 86 km and 90 km, using the same oxygen dissociation relations for altitudes below 90 km.

The Jacchia 77 model starts off with temperature $T_0 = 188$ K at altitude $z_0 = 90$ km to a temperature $T_X$ K at altitude $z_X = 125$ km with temperature gradient $G_X$ where $T_X$ is a function of the exospheric temperature $T_\infty$ as

$$T_X = T_0 + 110.5 \sinh^{-1}[0.0045(T_\infty - T_0)], \tag{3.86}$$

$$G_X = 1.9 \frac{T_X - T_0}{z_X - z_0}. \tag{3.87}$$

Then, the temperature can be obtained from the equations

$$T = T_X + \frac{T_X - T_0}{\pi/2} \tan^{-1}\left\{\frac{G_X}{\frac{(T_X - T_0)}{(\pi/2)}}(z - z_X)\left[1 + 1.7\left(\frac{z - z_X}{z - z_0}\right)^2\right]\right\}, \tag{3.88}$$

for z $< z_X$ and

$$T = T_X + \frac{T_\infty - T_X}{\pi/2} tan^{-1}\left\{\frac{G_X}{\frac{(T_\infty - T_X)}{(\pi/2)}}(z - z_X)[1 + 5.5 \times 10^{-5}(z - z_X)^2]\right\}, \tag{3.88}$$

for z $> z_X$, asymptotically approaching $T_\infty$.

Then, the profile of mean molecular mass $\bar{M}'$ is calculated for altitudes ranging from 90 km to 100 km, which is given as

$$\bar{M}'^{(z)} = \sum_{n=0}^{5} c_n (z - 90)^n, \tag{3.89}$$

where

$$c_0 = 28.89122, \tag{3.90}$$
$$c_1 = -2.83071 \times 10^{-2}, \tag{3.91}$$
$$c_2 = -6.59924 \times 10^{-3}, \tag{3.92}$$
$$c_3 = -3.39574 \times 10^{-4}, \tag{3.93}$$
$$c_4 = +6.19256 \times 10^{-5}, \tag{3.94}$$
$$c_5 = -1.84796 \times 10^{-6}. \tag{3.95}$$

The density profile $\rho'$ can be obtained from the mean molecular mass by integrating the barometric equation given as

$$\frac{d\rho'}{\rho'} = \frac{T}{\bar{M}} d\left(\frac{\bar{M}\prime}{T}\right) - \frac{\bar{M}\prime g}{R^* T} dz, \tag{3.96}$$

where $T$ is the temperature profile obtained previously with $R^* = 8.31432 \times 10^3$ kgm(kg-mol)$^{-1}$K$^{-1}$ is the universal gas constant and $\rho'$ is fixed to a boundary value of $\rho'_0 = 3.43 \times 10^{-6}$ kgm$^{-3}$ at $z = 90$ km and $g$ is the acceleration due to gravity defined as

$$g = 9.80665 \left(1 + \frac{z}{R_e}\right)^2 \ \text{ms}^{-2}, \tag{3.97}$$

where $R_e = 6.356766 \times 10^6$ m is the radius of Earth in meters.

Then, the number density $N'$ is given as

$$N' = \frac{A\rho'}{\bar{M}'}, \tag{3.98}$$

where $A = 6.02217 \times 10^{26}$ mks is the Avogradro's number. The number density $\mathrm{n}(N_2)$, $\mathrm{n}(Ar)$, $\mathrm{n}(He)$ is given as

$$\mathrm{n}(i) = q_0(i)\frac{\bar{M}'}{\bar{M}'_0}, \tag{3.99}$$

where $q_0(i)$ is the fraction by volume, and the number density $\mathrm{n}(O)$ and $\mathrm{n}(O_2)$ is given as

$$\log \mathrm{n}(O) = \log \mathrm{n}'(O) + \Delta \log \mathrm{n}'(O), \tag{3.100}$$
$$\log \mathrm{n}(O_2) = \log \mathrm{n}'(O_2) + \Delta \log \mathrm{n}'(O_2), \tag{3.101}$$

where

$$n'(O) = 2N'\left(1 - \frac{\bar{M}'}{\bar{M}'_0}\right), \tag{3.102}$$

$$n'(O_2) = N'\left\{\frac{\bar{M}'}{\bar{M}'_0}[1 + q_0(O_2)]\right\}, \tag{3.103}$$

$$\Delta \log n'(O) = -0.24e^{-0.009(z-97.7)^2}, \tag{3.104}$$

$$\Delta \log n'(O_2) = -0.07\{1 + \tanh[0.18(z - 111)]\}, \tag{3.105}$$

The $q_0(i)$ values are given as in Table 8 [Jacchia, 1977, Table 3].

**Table 8** Assumed sea-level composition [Jacchia, 1977, Table 3]

| Constituent | Fraction by volume |
|---|---|
| Nitrogen ($N_2$) | 0.78110 |
| Oxygen ($O_2$) | 0.20955 |
| Argon ($Ar$) | 0.009343 |
| Helium ($He$) | 0.000005242 |

For altitudes above 100 km, $N$ and ρ are computed by integrating the diffusion equation. The equation is given as

$$\frac{dn(i)}{n(i)} + \frac{dT}{T}(1 + \alpha_i) + \frac{dz}{H_i} + \frac{\Phi_i}{D}\frac{dz}{n(i)} = 0, \tag{3.106}$$

where $\alpha_i$ is the thermal diffusion coefficient, $\Phi_i$ is the vertical flux, $D$ is the mutual diffusion coefficient, and $H_i$ is the scale height. The diffusion coefficient is assumed to be zero, except for helium ($\alpha_{He} = -0.38$) and hydrogen ($\alpha_H = -0.25$) and the vertical flux is assumed to be all zero except for hydrogen, which is proportional to the number density of hydrogen at 500 km given as

$$\log_{10} n_{500}(H) = 5.94 + 28.9T_\infty^{-1/4} \text{ mks}, \tag{3.107}$$

$$\log_{10} \Phi(H) = 6.90 + 28.9T_\infty^{-1/4} \text{ mks}. \tag{3.108}$$

The scale height is given as

$$H_i = \frac{R^*T}{M_i g}, \tag{3.109}$$

and the diffusion coefficient is given as

$$D = 2.0 \times 10^{20} \frac{\sqrt{T}}{N}, \tag{3.110}$$

where $N$ is the total number density.

# 4. Initial CubeSat Design

A CubeSat consists of structure, thermal, OBDH (onboard data handling), TT&C (telemetry, tracking, and command), ADC (attitude determination and control), and electrical power subsystems. This chapter introduces each subsystem, and an initial design aid tables are proposed assuming that the subsystems will be purchased or that it can be designed and manufactured with similar specifications.

## 4.1 Structure

CubeSat structure is normally manufactured using aluminum Al6061 or Al7075 [California Polytechnic State University, 2009, p. 9] due to the thermal expansion coefficient of the CubeSat deployer. If the thermal expansion coefficient is not matched with the deployer, the CubeSat might get stuck. However, a drawback exists when selecting a similar material for the CubeSat structure as the deployer due to cold welding. Therefore, CubeSat structure is hard anodized after being manufactured in order to solve thermal expansion coefficient and cold welding problems. Furthermore, since CubeSats are limited in mass, structure must be carefully designed to minimize its mass while it withstands the impact and vibration from the launch.

Initial design aid table for structure is given as structure mass of ISIS (Innovative Solutions In Space), CubeSat Kit, and of SNUSAT (Seoul National University Satellite). Note that the mass in Table 9 does not include mounting elements, and thus a margin of 10~20% should be included.

**Table 9** Structure mass (in grams) for given CubeSat units

| | ISIS | CubeSat Kit | SNUSAT |
|---|---|---|---|
| 1U | 100 | 158 | - |
| 2U | 200 | 229 | 275 |
| 3U | 300 | 300 | - |

## 4.2 Thermal

The purpose of thermal subsystem is to keep the temperature of the satellite for certain components within a required level [Aguirre, 2013, p. 29]. Some components, for example batteries or microprocessors, may be critical to temperature in operating range or sensitive to temperature in mission performance such as optical lenses. However, use of optics or temperature sensitive components is uncommon for CubeSats. Some operation temperature ranges for common CubeSat components are given in Table 10.

**Table 10** Operation temperature ranges for common CubeSat components

| Component | Temperature range |
|---|---|
| Solar panel | $-40℃ \sim 85℃$ |
| Electrical Power Subsystem | $-40℃ \sim 85℃$ |
| Telemetry, Tracking, and Command | $-20℃ \sim 50℃$ |
| Batteries | $-10℃ \sim 50℃$ |
| Selected actuator (magnetorquer) | $-40℃ \sim 70℃$ |
| Selected sensor (sun sensor) | $-25℃ \sim 50℃$ |
| Onboard Computer | $-40℃ \sim 85℃$ |

Various studies such by Friedel et al. [2011], Dinh [2012] or Ecole Polytechnique Federale de Lausanne [2008] show space flight or simulation results that most CubeSat components come within thermal range for extreme cold or hot cases. However, some of the sensitive components such as batteries may lie in critical cases, and thus further analysis and individual thermal control should be considered. This study assumes that CubeSat components are well in range of the thermal range for phase-A, unless the mission requires specific requirements.

## 4.3 Onboard Data Handling

Onboard Data Handling subsystem works as a center for a satellite. The Onboard Data Handling subsystem tracks the status of the components checking the health of the satellite, known as housekeeping. Conventional CubeSats, due to low power available, used low-bit, low-performance processors for the onboard computer.

As CubeSats are utilized in low Earth orbit in altitudes lower than 1,000 km, radiation is not as of a big problem for the CubeSats, since the orbit is beneath the van Allen radiation belt. Also, as technology developed that high-bit processors now maintain low power as low-bit processors, e.g. ARM Cortex-M3, high-bit processors are beginning to be used for CubeSat onboard computer processors. Table 11 shows specifications of selected onboard computers.

**Table 11** Selected onboard computer specifications

| | GomSpace | CubeSat Kit | CubeSat Kit |
|---|---|---|---|
| Processor bit | 32 bit | 16 bit | 16 bit |
| Mass | 55 g | 88 g | 94 g |
| Volume | 0.1U | 0.13U | 0.13U |
| Clock | 8-40 MHz | 7.4 MHz | 32 MHz |
| Power | 120-230 mW | 20 mW | 70 mW |

## 4.4 Telemetry, Tracking, and Command

Telemetry, Tracking, and Command subsystem of a CubeSat is in charge of communication. CubeSat uses the amateur frequency band, which is allocated throughout the radio frequency spectrum. CubeSat commonly uses Very High Frequency (VHF) and Ultra High Frequency (UHF) for downlink and uplink. Recently, S-band and X-band are being demonstrated for CubeSats. Table 12 and Table 13 list specifications for Telemetry, Tracking, and Command subsystems and antennas.

**Table 12** Selected TT&C board specifications

| | | GomSpace | ISIS | ISIS | F'SATI |
|---|---|---|---|---|---|
| Mass | | 75 g | 85 g | 62 g | 80 g |
| Volume | | 0.18U | 0.15U | 0.15U | 0.12U |
| Frequency | Uplink | 435-438 MHz | 400-450 MHz | - | - |
| | Downlink | half-duplex | 130-160 MHz | 2.1-2.5 GHz | 2.4-2.48 GHz |
| Baud rate | Uplink | 4.8 kbps | 1.2 kbps | - | - |
| | Downlink | 9.6 kbps | 9.6 kbps | 100 kbps | 2 Mbps |
| RF power | | 30-34 dBm | 22 dBm | 28 dBm | 30 dBm |
| Power | | 2-5 W | 1.7 W | 3.5 W | 5.5 W |

**Table 13** Antenna specifications

| | CPUT | ISIS | GomSpace |
|---|---|---|---|
| Mass | 50 g | 100 g | 30 g |
| Volume | 0.04U | 0.07U | 0.02U |
| Frequency | 2.4-2.483 GHz | 400-450 MHz | 400-480 MHz |
| | - | 130-160 MHz | - |

## 4.5 Attitude Determination and Control

Attitude Determination and Control is required for stabilization, optimal ground link, mission requirements, or for survival. Attitude Determination and Control consists of determining part and controlling part [Aguirre, 2013, p. 31]. The determining part requires sensors to sense the attitude of the satellite, whereas the controlling part requires actuators to control the attitude of the satellite. Various sensors and actuators exist for CubeSats. Sun sensors, magnetorquers, and MEMS gyroscopes are common as sensors, and magnetometers and reaction wheels are common as actuators.

In this study, the performance of common sensors and actuators are evaluated for different size CubeSats, assuming the mass is evenly distributed along the CubeSat. The magnetorquer is assumed to be ISIS Magnetorquer Board and the reaction wheel is assumed to be Astrofein RW1. Note that magnetorquers can be also mounted into the solar panels.

**Table 14** Magnetorquer and reaction wheel specifications

| | Magnetorquer | Reaction Wheel |
|---|---|---|
| Mass | ~ 195 g | ~ 65 g |
| Volume | ~ 0.15 units | ~ 0.3 units |
| Maximum Torque | $4.2 \times 10^{-6} \sim 1.3 \times 10^{-5}$ Nm | $2.3 \times 10^{-5}$ Nm |
| Power Consumption | 0.24 ~ 0.48 W | 0.4 ~ 0.72 W |

**Table 15** Comparison between magnetorquer and reaction wheel performance

| | Moment of Inertia [kgm$^2$] | | Angular Acceleration [rads$^{-2}$] | |
|---|---|---|---|---|
| | | | Magnetorquer | Reaction Wheel |
| 1U | $I_{xx} = I_{yy}$ | 0.002217 | 0.005864 | 0.010374 |
| | $I_{zz}$ | 0.002217 | 0.005864 | 0.010374 |
| 2U | $I_{xx} = I_{yy}$ | 0.011083 | 0.001173 | 0.002075 |

| | | | | |
|---|---|---|---|---|
| | $I_{zz}$ | 0.004433 | 0.002933 | 0.005188 |
| 3U | $I_{xx} = I_{yy}$ | 0.033333 | 0.00039 | 0.000690 |
| | $I_{zz}$ | 0.006667 | 0.00195 | 0.003450 |

Note that magnetorquer is assumed for maximum Earth magnetic field.

**Table 16** Sun sensor and magnetometer specifications

| | Sun sensor | | Magnetometer |
|---|---|---|---|
| | Fine | Coarse | |
| Mass | 35 g | 5 g | 165 g |
| Accuracy | $\pm 0.1°$ | $\pm 0.5°$ | 10nT Sensitivity |
| Power Consumption | 0.2 W | 0.05 W | 400 mW |

Note that the numbers above are only from the hardware specification. For improved performance, sensor filters and control algorithms must be applied.

## 4.6 Electrical Power Subsystems

For the Electrical Power Subsystem of a CubeSat include the solar panels, the batteries, and the EPS board itself that performs regulation and distribution [Aguirre, 2013, p. 33]. EPS (e.g. Clyde-Space CubeSat 1U Electronic Power System) must generate power used for the CubeSat, store unused power and provide the required bus lines that other CubeSat components require, such as 3.3 V or 5 V bus.

In this study, the power generation and power storage capability for different CubeSat sizes are summarized. Note that solar panels are assumed to be attached to the side walls, thus deployable solar panels may increase power generation.

**Table 17** Power generation capability of CubeSats

| | Power Generation/panel | Mass/panel |
|---|---|---|
| 1U | 2.1 W | 42 g |
| 2U | 5.2 W | 69 g |
| 3U | 7.3 W | 135 g |

**Table 18** EPS board (Clyde-Space)

| Capacity | Volume | Mass |
|---|---|---|
| No batteries | 0.13U | 86 g |
| 10 Whr | 0.16U | 169 g |
| 20 Whr | 0.22U | 237 g |

**Table 19** EPS board (GomSpace)

| Capacity | Volume | Mass |
|---|---|---|
| No batteries | 0.16U | 105 g |
| ~20 Whr | 0.26U | 200 g |

In order to obtain power simulation results, operation analysis must be performed with power generation and power consumption modeled, which is performed using methods from chapter 3 and chapter 4 and shown in chapter 5.

# 5. Application on SNUSAT-1

The initial design approach and feasibility check through operation analysis is performed on SNUSAT-1, with the scenario set for the QB50 project. The QB50 project is a lower thermosphere exploration and Earth re-entry project where 50 CubeSats are deployed at the same time, performing multi-point, in-situ, long-duration measurements of the key constituents of the atmosphere at altitudes of 90-320 km. This chapter sets some of the top-level requirements, with initial design approached using the tables given in chapter 2.

## 5.1. Top-Level Requirements

The top-level requirements of SNUSAT-1 can be categorized as space segment requirements, ground segment requirements and launch segment requirements [NASA, 2007, p. 41]. Top-level requirements are the critical requirements that will not change throughout the design process. Each segment will be defined by mission requirements, CubeSat requirements, or resource limitations.

### 5.1.1. Space Segment Requirements

The space segment requirements are directly related to the CubeSat. SNUSAT-1 has total four missions which are low thermosphere exploration, Fault Detection Isolation and Recovery (FDIR) algorithm verification, CubeSat drag coefficient modeling, and demonstration of COTS camera for future use. The low thermosphere exploration mission is the user defined QB50 project mission. Some of the top-level requirements are given as Table 20.

**Table 20** Top-level space segment requirements of SNUSAT-1

| Subsystem | Requirements |
|---|---|
| Structure | Double unit CubeSat |
| | Mass limited to 2 kg |
| ADCS | Commissioning within 2 days |
| | Z-axis aligned with the ram direction |

| | |
|---|---|
| | Pointing accuracy of $\pm 5°$ (TBC) |
| | Pointing knowledge of $\pm 1°$ (TBC) |
| | Redundant sensor/actuator for FDIR |
| EPS | 3.3V and 5V power bus |
| TT&C | At least 1-2 Mbit data downlinked per orbit |
| | VHF downlink/UHF uplink |
| OBC | At least 2 Mbit data will be daily stored |
| | I2C bus |
| Orbit | Circular orbit at 320 km altitude, 79° inclination |

### 5.1.2. Ground Segment Requirements

Ground segment requirements are the requirements directly related with the ground station. The ground segment requirements may be set from special needs of high-gain antennas for deep space communication. In the case for SNUSAT-1, the ground segment requirements are set from the use of Global Educational Network for Satellite Operations (GENSO) system. The requirements are given as Table 21.

**Table 21** Top-level ground segment requirements of SNUSAT-1

| Requirements |
|---|
| The ground station should be GENSO compatible |
| The ground station must be registered |
| International Telecommunication Union (ITU) rules must be obeyed |

### 5.1.3. Launch Segment Requirements

Launch segment requirements define the requirements that must be met for the satellite to safely go out to the space. Conventionally, CubeSats have been launched as piggy-backs of other main payload, thus additional requirements from the main payload needed to be considered. However, a whole launcher is planned to be used just for the QB50 project, and thus only the launcher requirements are considered. The requirements are given as Table 22.

**Table 22** Top-level launch segment requirements of SNUSAT-1

| Requirements |
|---|
| Tolerable deformation and deployables must be held together |
| Outgassing check must be performed at $5 \times 10^{-4}$ Torr |

| |
|---|
| Thermal vacuum baking must be performed |
| If the launcher is not specified refer to GSFC-STD-7000 |

## 5.2. Initial Design Approach

The initial design is approached by looking up the tables in chapter 2. Some of the design parameters are given from mission requirements such as the payload mass, payload power consumption, payload volume, and payload data rate. The payload specification is given in the next tables with 20% margin included.

**Table 23** QB50 payload specification

| Parameter | Specification |
|---|---|
| Mass | 600 g |
| Volume | 0.6U |
| Power | 600 mW |
| Data rate | 2.4 Mbit/day |

Also, from the FDIR mission requirements, the redundant sensors and actuators are targeted for two MEMS gyroscopes and a 4-axis reaction wheel. Taking the mission requirements under consideration and 2U CubeSat requirements, two options for the mass and volume budget are given as Table 24.

The margin includes mass for spacers, harnesses, and uncertainties. Solar panel mounted magnetorquers are used for X-axis and Y-axis. The ADCS board includes a Z-axis magnetorquer, three sun sensors, a GPS, a Camera, and two Inertial Measurement Unit (IMU), which includes a three-axis gyroscope, a three-axis accelerometer and a three-axis magnetometer. Note that the first option uses half-duplex transceiver, and the second option uses 10 Whr batteries due to the 2 kg mass constraints.

The power budget is obtained for the two options, configuration-A being the top and configuration-B being the bottom, with operation conditions, which are given as Table 25.

Feasibility of the SNUSAT-1 will be assessed according to the initial design approach, using the numerical methods and models described in chapter 2 and chapter 3.

**Table 24** Mass and volume budget for SNUSAT-1

| System | Description | Model | spec mass [g] | margin | total mass [g] | volume [U] |
|---|---|---|---|---|---|---|
| **ADCS** | ADCS Board | Sun-sensor/Gyros/GPS/Magnetometer/Magnetorquer/Camera | 160 | 20% | 192 | 0.3 |
| | Reaction Wheel | Tetrahedron Set | 150 | 10% | 165 | 0.5 |
| **EPS** | EPS Board | NanoPower P31U Electronic Power System | 200 | 10% | 220 | 0.26 |
| | Solar Panel | CS 2-Unit CubeSat Side Solar Panel with magnetorquers | 328 | 10% | 360.8 | |
| **Communication** | Transciever | NanoCom U482C | 75 | 10% | 82.5 | 0.18 |
| | Antenna | UHF Turnstile Antenna | 30 | 20% | 36 | |
| **Structure** | Structure | 2-Unit CubeSat Structure | 200 | 15% | 230 | |
| **OBC** | Onboard Computer | NanoMind A712 v1.5 On Board Computer | 55 | 10% | 60.5 | 0.1 |
| **Science Sensor** | Science Sensor | VKI Science Sensor | 500 | 20% | 600 | 0.6 |
| **Total** | | | **1698** | | **1946.8** | **1.94** |

| System | Description | Model | spec mass [g] | margin | total mass [g] | volume [U] |
|---|---|---|---|---|---|---|
| **ADCS** | ADCS Board | Sun-sensor/Gyros/GPS/Magnetometer/Magnetorquer/Camera | 160 | 20% | 192 | 0.3 |
| | Reaction Wheel | Tetrahedron Set | 150 | 10% | 165 | 0.5 |
| **EPS** | EPS Board | 2U CubeSat EPS with 10Whr batteries | 169 | 10% | 185.9 | 0.16 |
| | Solar Panel | CS 2-Unit CubeSat Side Solar Panel with magnetorquers | 328 | 10% | 360.8 | |
| **Communication** | Transciever | VHF downlink/UHF uplink Full Duplex Transceiver | 85 | 10% | 93.5 | 0.15 |
| | Antenna | Dipole Configuration Deployable Antenna System | 100 | 10% | 110 | |
| **Structure** | Structure | 2-Unit CubeSat Structure | 200 | 15% | 230 | |
| **OBC** | Onboard Computer | NanoMind A712 v1.5 On Board Computer | 55 | 10% | 60.5 | 0.1 |
| **Science Sensor** | Science Sensor | VKI Science Sensor | 500 | 20% | 600 | 0.6 |
| **Total** | | | **1747** | | **1997.7** | **1.81** |

**Table 25** Power budget for SNUSAT-1

| System | Description | Model | spec power [mW] | condition |
|---|---|---|---|---|
| **ADCS** | ADCS Board | Sun-sensor/Gyros/Magnetometer/Accelerometer | 355 | nominal |
| | | Sun-sensor/Gyros/Magnetometer/Accelerometer | 230 | low power mode |
| | | GPS | 500 | nominal |
| | | Magnetorquer | 200 | on operational |
| | | Camera | 60 | on operational |
| | Reaction Wheel | Tetrahedron Set Standby | 400 | |
| | | Tetrahedron Set fully operational | 1680 | on operational |
| **EPS** | EPS Board | NanoPower P31U Electronic Power System | 200 | nominal |
| | Solar Panel | CS 2-Unit CubeSat Side Solar Panel with magnetorquers | 400 | on operational |
| **Communication** | Transciever | NanoCom U482C Transmitting | 5000 | on operational |
| | | NanoCom U482C Receiving | 500 | on operational |
| | | NanoCom U482C Standby | 230 | nominal |
| **OBC** | Onboard Computer | NanoMind A712 v1.5 On Board Computer | 230 | nominal |
| **Science Sensor** | Science Sensor | VKI Science Sensor | 600 | nominal |

| System | Description | Model | spec power [mW] | condition |
|---|---|---|---|---|
| **ADCS** | ADCS Board | Sun-sensor/Gyros/Magnetometer/Accelerometer | 355 | nominal |
| | | Sun-sensor/Gyros/Magnetometer/Accelerometer | 230 | low power mode |
| | | GPS | 500 | nominal |
| | | Magnetorquer | 200 | on operational |
| | | Camera | 60 | on operational |
| | Reaction Wheel | Tetrahedron Set Standby | 400 | nominal |
| | | Tretrahedron fully operational | 1680 | on operational |
| **EPS** | EPS Board | 2U CubeSat EPS with 10Whr batteries | 200 | nominal |
| | Solar Panel | CS 2-Unit CubeSat Side Solar Panel with magnetorquers | 400 | on operational |
| **Communication** | Transciever | VHF downlink/UHF uplink Full Duplex Transceiver Transmitting | 1550 | on operational |
| | | VHF downlink/UHF uplink Full Duplex Transceiver Receiving | 200 | on operational |
| **OBC** | Onboard Computer | NanoMind A712 v1.5 On Board Computer | 230 | nominal |
| **Science Sensor** | Science Sensor | VKI Science Sensor | 600 | nominal |

## 5.3. Feasibility Assessment

SNUSAT-1 feasibility is assessed according to data transmission, power, and lifetime. The operation scheme is given as Figure 6.

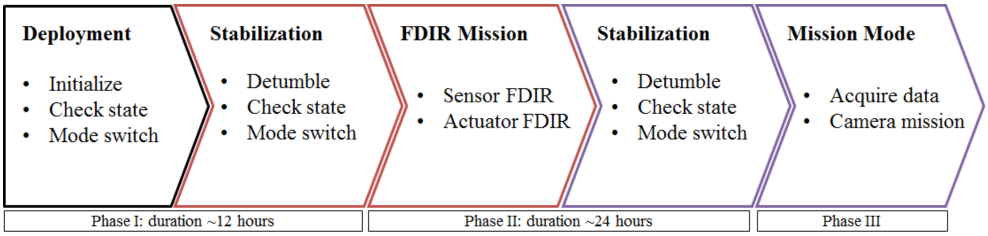


**Figure 6** Operation scheme of SNUSAT-1

On deployment, SNUSAT-1 will be on standby for status checkup while power is generated (safe mode). After SNUSAT-1 finishes checkup and the power level is adequate, it commences the detumble algorithm and stabilizes for nominal mode. During the second phase, FDIR mission is performed. First, sensor FDIR is performed on the MEMS gyroscope and then, actuator FDIR is performed on the reaction wheels. At end of FDIR mission, SNUSAT-1 commences the detumble algorithm, stabilizing into nominal mode for phase three. As the QB50 requirement phase two ends within 48 hours and science sensors acquire data as phase three starts. Saved data is downloaded upon request (TBC), while specific Earth observation missions are uploaded for the camera.

In this study, a virtual ground station is located in Seoul National University, and data is transmitted with a $10°$ cutoff angle. It is assumed that magnetorquers are used for detumbling, and reaction wheels are used for nominal mode attitude control. The initial orbit element parameters are given in Table 26.

**Table 26** Initial orbit element parameters of SNUSAT-1

| Parameter | Value |
|---|---|
| Semimajor axis | 6698.137 km |
| Eccentricity | 0 |
| Inclination | 79° |
| Right ascension of the ascending node | 0° |
| Argument of periapsis | 0° |
| True Anomaly | 0° |

### 5.3.1. Lifetime

As introduced in the previous chapters, atmospheric drag depends on the exospheric temperature, and thus lifetime also depends on the exospheric temperature. The lifetime is simulated for various exospheric temperatures, as shown in Figure 7.

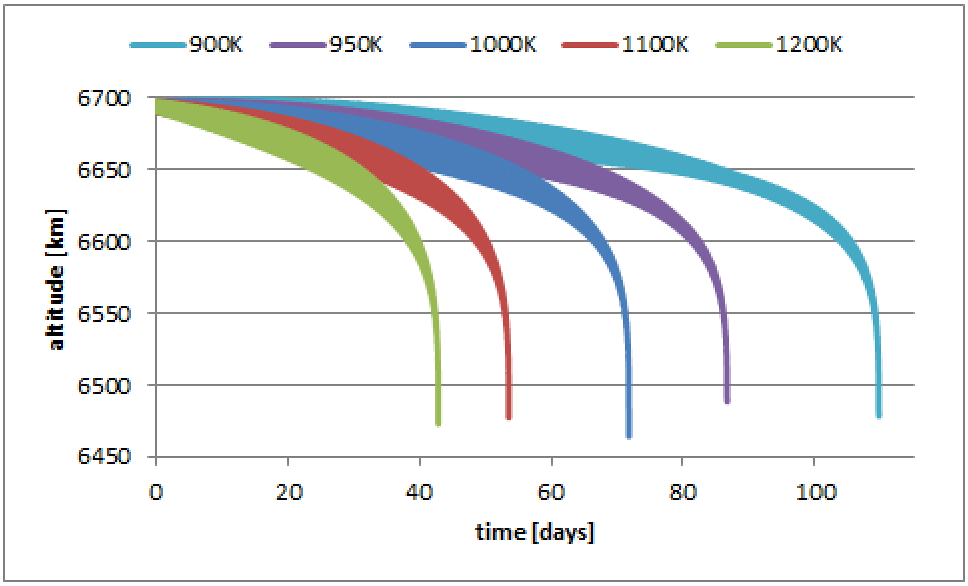


**Figure 7** Lifetime of SNUSAT-1 depending on exospheric temperature

In this study, feasibility test is performed for the exospheric temperature of 950 K, in which the satellite lifetime is near 90 days, because 90 days is the mission scenario of the QB50 project. Therefore, this assumption is made also to check the feasibility for a 90 days operation condition.

### 5.3.2. Link Analysis

Regarding the link margin, it can be calculated as [Wertz, 2008, pp.550-567] in Table 27. It can be seen that the link margin is enough for all TT&C boards.

Link time can be obtained by setting a circular region around the ground station. Boundary conditions of link conditions are given for the norm of satellite and ground station longitude and latitude, with a $10°$ cutoff angle. From the operation condition set as in section 5.3.1., the link status is shown as in Table 28.

**Table 27** Link margin of SNUSAT-1 for 22dBm transmission

| Category | Item | Value | Unit |
|---|---|---|---|
| Transmitter | Transmit Power | -8.00 | dBW |
| | Line Loss | -1 | dB |
| | Antenna Gain | 0 | dB |
| Environment | Space Loss | -135.2 | dB |
| | Atmosphere Loss | -0.3 | dB |
| | Rain Loss | -1 | dB |
| | Polarization Loss | -3 | dB |
| Receiver | Antenna Gain | 10 | dBi |
| | Line Loss | -0.3 | dB |
| | Pointing Loss | -1 | dB |
| | System Noise | -23.4 | dBK |
| Required | Eb/No | -10 | dB |
| | Data Rate | -39.82 | dBHz |
| | Bit Error | -4 | dB |
| | Boltzmann | 228.6 | dBW/(HzK) |
| Margin | | 11.58 | dB |

**Table 28** Link status for SNUSAT-1

| Total link time | Average link time | Average revisit time |
|---|---|---|
| 30,555 seconds | 226.3 seconds | 54814.8 seconds |

According to the TT&C specifications, downlink rate is assumed to be 9600 bps. Then, data transmission is equal to 3.26 Mbps daily downlink, which gives a 60% margin. However, link analysis assumes link neglecting the power level of SNUSAT-1. Therefore, for a more realistic operation simulation, power constraints must be considered.

### 5.3.3. Power

Power simulation is performed according to the power budget. Assumptions are 12 hours detumbling, which uses magnetorquers, and reaction wheel use for nominal mode. The actuators are assumed fully operational. Power loss due to efficiency is neglected, and battery charge is assumed to be linear throughout. The Z-axis is assumed to be aligned with the ram direction and the X-axis is assumed to be aligned with the position vector. Power simulation is performed for initial design cases of configuration-A and configuration-B.

The results for configuration-A for short-term initial deployment sequence and long-term operational sequence is shown as in Figure 9 and Figure 10 and the results for configuration-B for short-term initial deployment sequence and long-term operational sequence is shown as in Figure 11 and Figure 12. Due to power, configuration-A transmission occurs only 8,308 seconds, which is 27% of the link time, and configuration-B transmission occurs only 12,953 seconds, which is 42.3% of the link time.

**Table 29** Reaction wheel specification of Astrofein RW1

| Parameter | Value |
|---|---|
| Angular momentum (8,000 rpm) | $5.8 \times 10^{-4}$ Nms |
| Nominal torque | $23 \times 10^{-6}$ Nm |
| Moment of inertia | $7.0 \times 10^{-7}$ kgm$^2$ |
| Power consumption (8000 rpm) | $\leq$ 0.62 W |

For both cases, the power level drops down to safe mode for long-term operational sequence. Thus, either a more accurate prediction of power budget is required for actuators. Since the numerical code used for this study does not embed a controller, the power budget for the actuator must be further predicted. The reaction wheel specification is further given as Table 29.

Then, neglecting external disturbance and friction of the reaction wheel, the angular momentum $\Omega_b$ required for a circular orbit with radius $r$ can be assumed as

$$\Omega_b = I_b \omega_b = I_w \omega_w, \tag{5.1}$$

$$\omega_b = 2\pi / \left(2\pi r / \sqrt{\mu / r}\right), \tag{5.2}$$

where the moment of inertia of the satellite $I_b = 0.00833$ kgm$^2$, rotation speed of the satellite $\omega_b = 0.00115$ rads$^{-1}$, and the moment of inertia of the wheel $I_w = 7.0 \times 10^{-7}$ kgm$^2$. Then, the rotation speed of the reaction wheel required $\omega_w = 13.711$ rads$^{-1}$ or $\omega_w = 130.93$ rpm. Therefore, we may further assume that equivalent wheel rotation power consumption of 8,000 rpm is capable of controlling the satellite attitude, which is 0.62 W.

Further introducing a 1U size solar panel on the -Z-axis (+Z-axis must be revealed), a 2.1 W solar panel with 42 g can be assembled for additional power generation. The reconfigured case long-term operational sequence analysis is shown in Figure 13 and Figure 14. Reconfigured configuration-A transmission time is 24,971 seconds, which is 81.7% of the link time, and reconfigured configuration-B transmission time is 26,813 seconds, which is 87.7% of the link time.

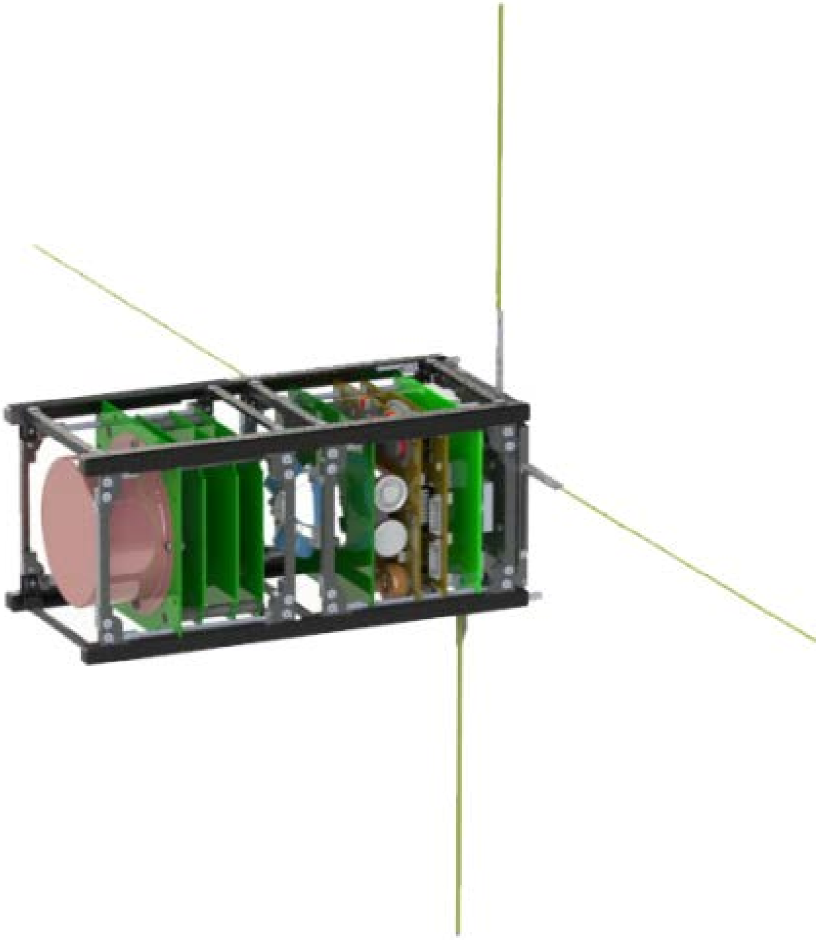

**Figure 8** 3D CAD render of SNUSAT-1

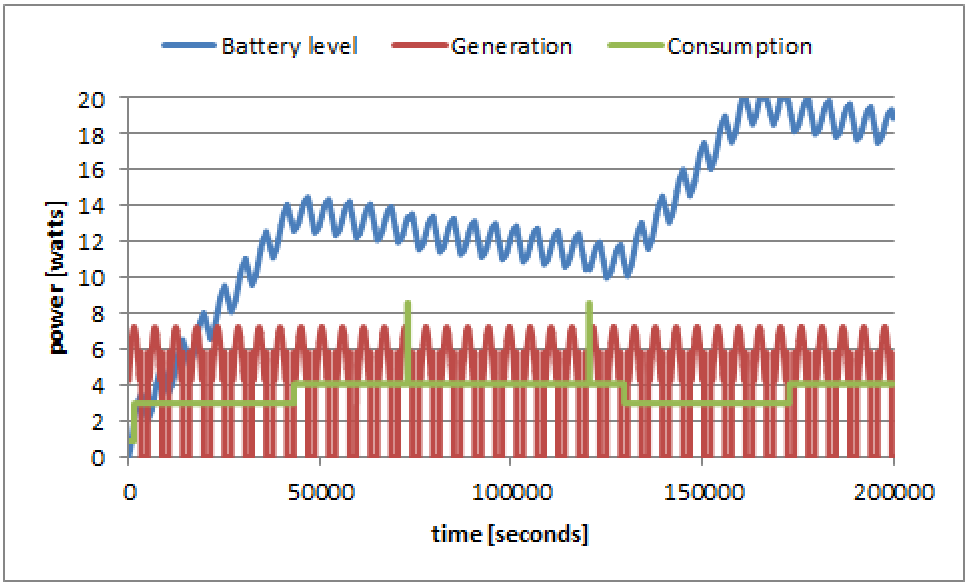


**Figure 9** Short-term power simulation of configuration-A

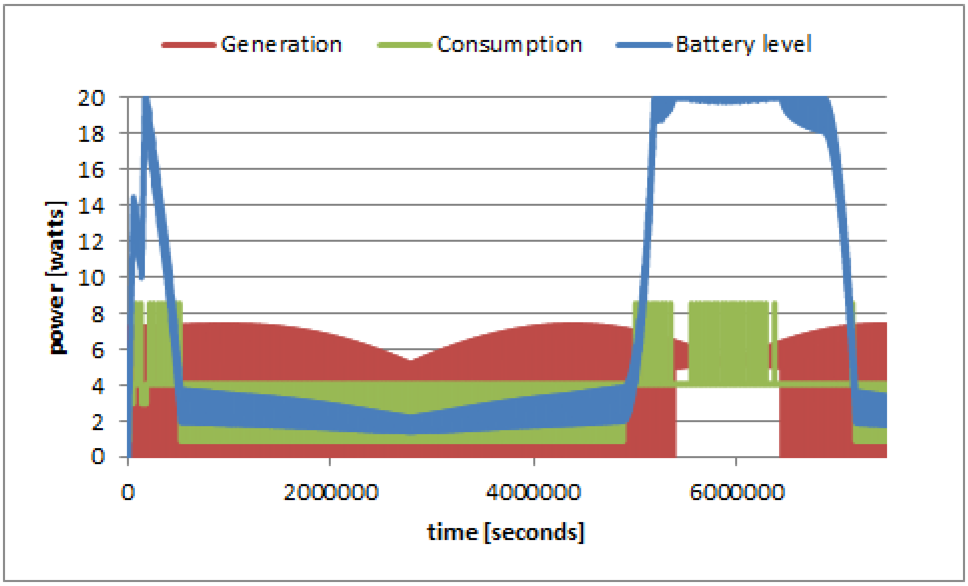


**Figure 10** Long-term power simulation of configuration-A

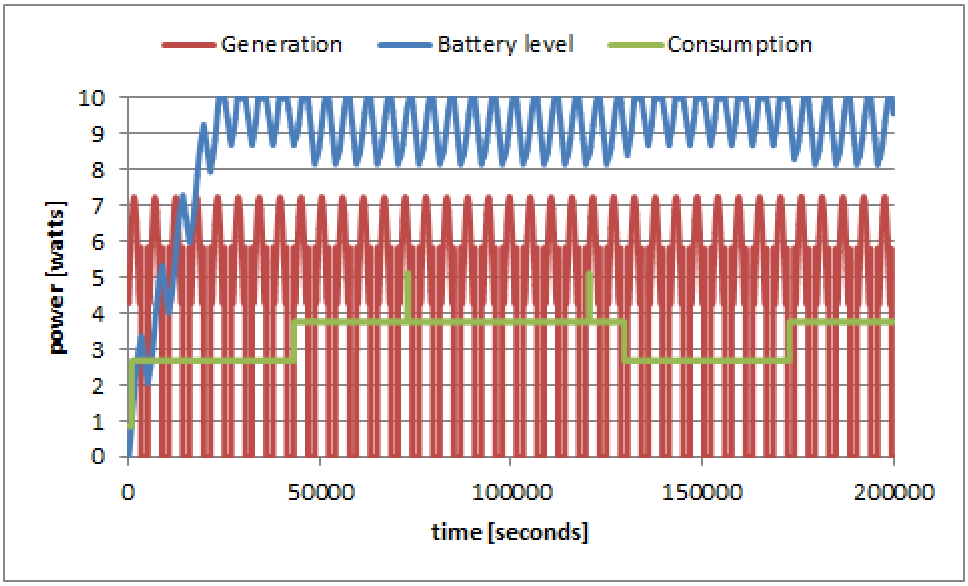


**Figure 11** Short-term power simulation of configuration-B

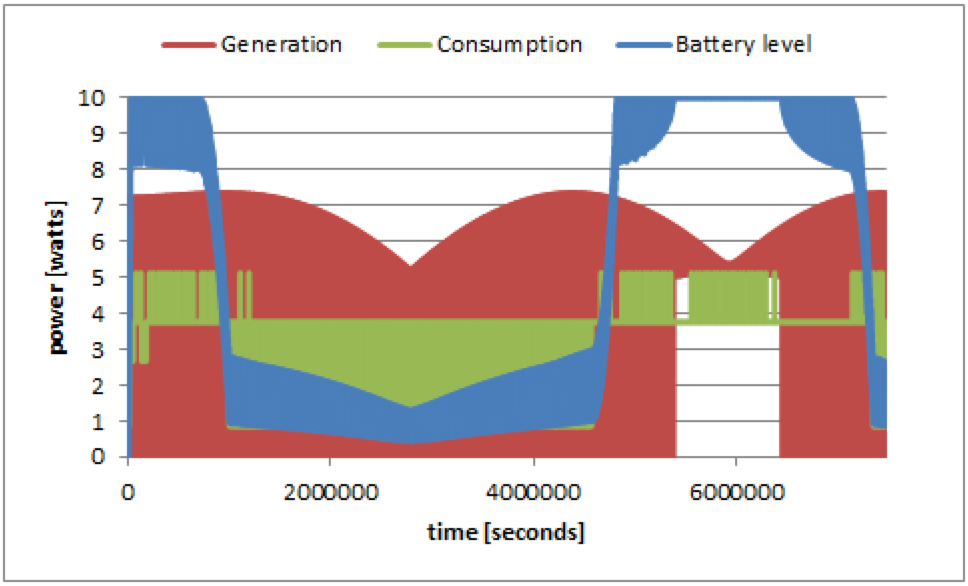


**Figure 12** Long-term power simulation of configuration-B

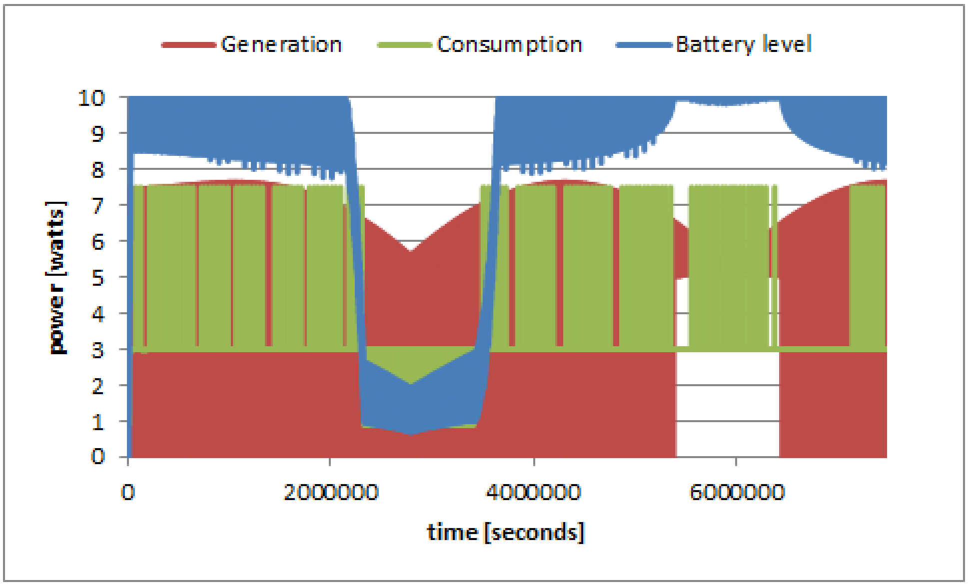

**Figure 13** Long-term power simulation of reconfigured configuration-A

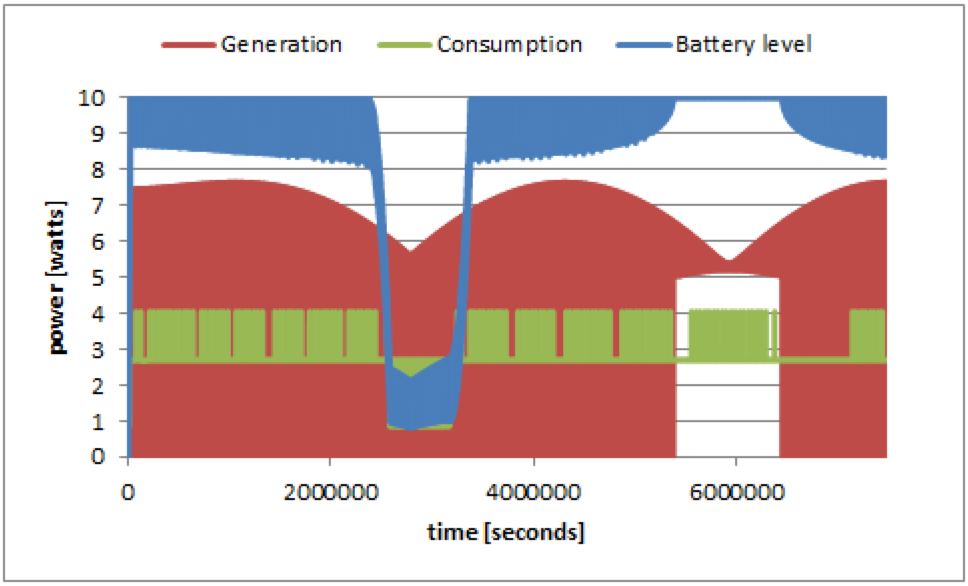

**Figure 14** Long-term power simulation of reconfigured configuration-B

# 6. Conclusion

This study focuses on the pre-phase A procedure of technically assessing a CubeSat project. Pre-phase A must be short, but adequate, for competing over successful proposals. By building up a systematic pre-phase A assessment tool, resource will be able to be allocated more efficiently.

In the beginning, basic method for numerically analyzing a satellite orbit and modeling the space environment is introduced. Cowell's method is used, considering perturbing acceleration due to geopotential, atmospheric drag, solar radiation pressure, and third body. The space environment is modeled for ephemerides, rotational elements, eclipse, and the atmospheric density.

Then, a baseline for initial design approach is given in tables for CubeSats, considering the fact that CubeSat is a standardized NanoSatellite. Although specific missions would require customized design, the mass and volume limitation of CubeSat and the efficiency or specific energy of solar cells and batteries allow a close initial design approach.

Given top-level requirements, it is possible to assess the feasibility of a project over the initial design. Initial design is performed for a double unit CubeSat, SNUSAT-1 for the QB50,

Two initial designs were suggested, and according to the analysis, transmission occurred only 27% and 42.3% of the link time, due to power limitation. Further assumption was made with basic dynamics for a more realistic power budget, and an additional bottom solar panel was assembled. According to the new assumption and the reconfigured design, transmission occurred for 81.7% and 87.7% of the link time. However, due to the mass limitation as shown in Table 30, the initial design allows 2.75 Mbps average daily data transfer, which gives a 37.5% margin.

Regarding the power results, at low power generation regions, SNUSAT-1 safe mode is activated, therefore it is suggested that high-power consuming components to low-power consuming components or the use of high-power consuming components usage is limited. Additionally, careful communication sequence plan is recommended that transmission is restricted for the low power generation regions, and instead data is continuously transmitted during the high power generation regions. Such solutions shall be further considered for later design procedures.

**Table 30** Reconfigured mass and volume budget for SNUSAT-1

| System | Description | Model | spec mass [g] | margin | total mass [g] | volume [U] |
|---|---|---|---|---|---|---|
| **ADCS** | ADCS Board | Sun-sensor/Gyros/GPS/Magnetometer/Magnetorquer/Camera | 160 | 20% | 192 | 0.3 |
| | Reaction Wheel | Tetrahedron Set | 150 | 10% | 165 | 0.5 |
| **EPS** | EPS Board | NanoPower P31U Electronic Power System | 200 | 10% | 220 | 0.26 |
| | Solar Panel | CS 1-Unit CubeSat Bottom Solar Panel | 42 | 10% | 46.2 | |
| | Solar Panel | CS 2-Unit CubeSat Side Solar Panel with magnetorquers | 328 | 10% | 360.8 | |
| **Communication** | Transciever | NanoCom U482C | 75 | 10% | 82.5 | 0.18 |
| | Antenna | UHF Turnstile Antenna | 30 | 20% | 36 | |
| **Structure** | Structure | 2-Unit CubeSat Structure | 200 | 15% | 230 | |
| **OBC** | Onboard Computer | NanoMind A712 v1.5 On Board Computer | 55 | 10% | 60.5 | 0.1 |
| **Science Sensor** | Science Sensor | VKI Science Sensor | 500 | 20% | 600 | 0.6 |
| **Total** | | | **1740** | | **1993** | **1.94** |

| System | Description | Model | spec mass [g] | margin | total mass [g] | volume [U] |
|---|---|---|---|---|---|---|
| **ADCS** | ADCS Board | Sun-sensor/Gyros/GPS/Magnetometer/Magnetorquer/Camera | 160 | 20% | 192 | 0.3 |
| | Reaction Wheel | Tetrahedron Set | 150 | 10% | 165 | 0.5 |
| **EPS** | EPS Board | 2U CubeSat EPS with 10Whr batteries | 169 | 10% | 185.9 | 0.16 |
| | Solar Panel | CS 1-Unit CubeSat Bottom Solar Panel | 42 | 10% | 46.2 | |
| | Solar Panel | CS 2-Unit CubeSat Side Solar Panel with magnetorquers | 328 | 10% | 360.8 | |
| **Communication** | Transciever | VHF downlink/UHF uplink Full Duplex Transceiver | 85 | 10% | 93.5 | 0.15 |
| | Antenna | Dipole Configuration Deployable Antenna System | 100 | 10% | 110 | |
| **Structure** | Structure | 2-Unit CubeSat Structure | 200 | 15% | 230 | |
| **OBC** | Onboard Computer | NanoMind A712 v1.5 On Board Computer | 55 | 10% | 60.5 | 0.1 |
| **Science Sensor** | Science Sensor | VKI Science Sensor | 500 | 20% | 600 | 0.6 |
| **Total** | | | **1789** | | **2043.9** | **1.81** |

# References

Aguirre M., *Introduction to Space Systems: Design and Synthesis*, Springer, 2013.

Bate R., Mueller D., White J., *Fundamentals of Astrodynamics*, New York: Dover Pulbications, Inc., 1971.

Bond V., Allman M., *Modern Astrodynamics: Fundamentals and Perturbation Methods*, New Jersey: Princeton University Press, 1996.

California Polytechnic State University, "CubeSat Design Specification," The CubeSat Program, 2009.

Bosch W., "On the Computation of Derivatives of Legendre Functions," Physics and Chemistry of the Earth, Vol. 25, No. 9-11, 2000, pp. 655-659.

Dinh D., "Thermal modeling of NanoSat," Master's Thesis, San Jose State University, 2012.

Ecole Polytechnique Federale de Lausanne, "Swisscube Thermal Analysis," Phase C Report, 2008.

Eshagh M., Abdollahzadeh M., "Simplification of geopotential perturbing force acting on a satellite," Artificial Satellites, Vol. 43, No. 2, 2008.

Friedel J. and McKibbon S., "Thermal Analysis of the CubeSat CP3 Satellite," Senior Project, California Polytechnic State University, 2011.

Hedin A., Spencer N., Killeen T., "Empirical global model of upper thermosphere winds based on atmosphere and dynamics explorer satellite data," Journal of Geophysical Research, Vol. 93, No. A9, 1988, pp. 9959-9978.

Holmes S.A., Featherstone W.E., "A unified approach to the Clenshaw summation and the recursive computation of very high degree and order normalised associated Legendre functions," Journal of Geodesy, Vol. 76, 2002, pp. 279-299.

Hwang C., and Lin M.-J., “Fast integration of low orbiter’s trajectory perturbed by the earth’s non-sphericity,” Journal of Geodesy, Vol. 72, 1998, pp. 578-585.

Jacchia L.G., “Thermospheric temperature, density, and composition: new models,” Smithonian Astrophysical Observatory, 1977.

Montenbruck O., Gill E., *Satellite Orbits: Models, Methods, and Applications*, Springer, 2000.

NASA, *NASA Systems Engineering Handbook*, NASA/SP-2007-6105 Rev1, 2007.

Press W., Teukolsky S., Vetterling W., Flannery B., *Numerical Recipes: The Art of Scientific Computing*, New York: Cambridge University Press, 2007.

Seidelmann P., Archinal B., A’hearn M., Conrad A., Consolmagno G., Hestroffer D., Hilton J., Krasinsky G., Neumann G., Oberst J., Stooke P., Tedesco E., Tholen D., Thomas P., Williams I., “Report of the IAU/IAG Working Group on cartographic coorinates and rotational elements: 2006,” Celestial Mechanics and Dynamical Astronomy, Vol. 98, 2007, pp. 155-180.

Vallado D., Finkleman D., “A Critical Assessment of Satellite Drag and Atmospheric Density Modeling,” AIAA/AAS Astrodynamics Specialist Conference, 2008.

Wertz J., Larson W., *Space Mission Analysis and Design*, New York: Springer, 2008.

# 초 록

본 논문은 큐브위성을 위한 초기 설계 접근 방법을 제시한다. 특히, pre-phase A의 기술적 적합성에 중점을 맞춰져 있다. Pre-phase A 과정은 성공적인 제안서와 프로젝트를 위해 매우 중요한 단계이다. 간단한 임무 분석 및 운영 모사 방법을 소개하고 이를 도표 기반 초기 설계 접근 방법과 접목시킴으로써 자원을 보다 효율적으로 분배할 수 있다.

운영 모사를 위해 지구 중력구배, 대기의 공기저항, 태양 복사압, 그리고 third body에 의한 섭동을 Cowell's method에 포함시켜 운동방정식을 세운다. 우주환경 모사를 위해 항성 위치 모델링, 항성 회전축 모델링, 식(蝕) 모델링, 그리고 대기 밀도 모델링 방법을 소개한다.

SNUSAT-1 초기설계를 위해 제안된 도표 기반 초기 설계와 최상위 요구사항을 통해 pre-phase A 기술적 적합성 평가를 수행한다.

주요어: 큐브위성, 초기설계, Pre-Phase A, 설계 도표, 임무 분석, 운용 모사
학 번: 2011-20709